UNMANNED AERIAL SYSTEMS (UAS) IN AGRICULTURE: DATA STABILITY AND UTILITY

A Dissertation Presented for the

Doctor of Philosophy

Degree

The University of Tennessee, Knoxville

Lori Allison Duncan

December 2019

Copyright © 2019 by Lori Allison Duncan
All rights reserved.

DEDICATION

To my daughter, Sawyer Kate:

No title I could ever earn will ever surpass being your mommy.

I dedicate this dissertation to you, my little wildflower.

ACKNOWLEDGEMENTS

I must begin by acknowledging and thanking Mike Buschermohle. Mike saw potential in me through my undergraduate education, graduate school for a master's degree, employment as an Extension professional, and then advised me through my doctoral studies. I am very thankful that I have had Mike as a colleague, a boss, a mentor, an advisor, and a friend. My other committee members – John Wilkerson, Willie Hart, and Tyson Raper – have been instrumental and steadfast in their support throughout my studies and I could not be here today without their guidance, assistance, and unfailing mentorship. I am indebted to my entire committee for the support and encouragement they provided through some very difficult and challenging times. As I pursued this degree under full-time employment, I would be remiss to not acknowledge my supervisors that provided encouragement throughout this process including the chancellor, deans, and my department head – Julie Carrier. Julie has been there to cheer me on and provide reassurance and guidance to me as a student, employee, and mother. Thank you to my colleagues in BESS, UTIA, and across the state who have motivated me to complete this degree so that I can follow in their exceptional footsteps, creating long-lasting impact in the lives and communities of Tennesseans.

Growing up, I had absolutely no idea what I wanted to do or who I wanted to be. I watched my parents and grandparents give their all at work and at home, all while maintaining the highest values and character. I knew I wanted to do the same. Thank you to my parents for motivating me and always believing in me. Most of all, thank you for providing an admirable example of what I wanted to be – a good, hardworking person. To my husband and best friend: none of this would be possible without you. You have endured daily whining, celebrating, stressing, and procrastinating for the last 6 years. You are the best father and did much more than your share of chores and parenting so that I could be a full-time employee, student, and mom. You even read and edited this dissertation and provided input on my research. I love you, and am so thankful our daughter can grow up with those expectations for her future spouse. I am also grateful and eternally inspired by our daughter, Sawyer Kate. Thank you for being patient when I had to work long hours, and thank you for always reminding me to be inquisitive and curious about the world around me.

ABSTRACT

The use of unmanned aerial systems (UAS) in production agriculture has exponentially increased in recent years due to their ability to acquire aerial imagery in a time and cost effective manner. Many producers and crop advisors use UAS as a platform to collect multispectral imagery that can be used to calculate a vegetation index (VI) map. These VI maps are then used to assess crop health and to make in-season management decisions on a spatial basis. Due to the surge in UAS adoption by non-experienced users as well as the sensitivity of potential management decisions to data quality, the first objective of this dissertation is to identify environmental attributes that impact the stability of VI maps derived from UAS-acquired data and develop recommendations for standard operating procedures. Specifically, these environmental factors include diurnal effects as well as shading from transient cloud cover. Analysis revealed that shadows cast by clouds can have a significant effect on normalized difference VIs, however these differences are not great enough to warrant a management change. However, the reflectance in individual bands is consistently and significantly affected by cloud cover. Also, a significant diurnal effect was observed in VIs and in the individual wavelengths. In order to fully realize benefits of low-cost technologies such as UAS and smartphones, the second objective is to identify image acquisition and post-processing techniques to enhance the utility of VI maps derived from smartphone and UAS-acquired data. Specifically, the objectives of this study were to evaluate the ability of early and late season ground-based measurements to provide insight into cotton nitrogen (N) status and to evaluate the ability of aerial-based measurements to correlate to ground-based measurements. This study demonstrates the usefulness of VIs developed from both UAS and smartphones in predicting in-season cotton N status.

TABLE OF CONTENTS

Chapter 1 – INTRODUCTION 1
1.1 Background 2
1.1.1 In-Field Spatial Variability and Variable Rate Technologies 2
1.2 Data Acquisition 4
1.2.1 Platforms 4
1.2.2 Spatial Resolution 4
1.2.3 Spectral Resolution 5
1.2.4 Radiometric Resolution 6
1.2.5 Temporal Resolution 6
1.2.6 Optimization of Resolutions 7
1.2.7 Calibration 7
1.3 Vegetation Indices 8
1.3.1 Applications 10
1.4 Potential UAV Data Quality and Stability Issues 10
1.5 Objectives 11
1.5.1 Dissertation Composition 11
1.6 References 13
Chapter 2 - EFFECT OF CLOUD COVER ON VEGETATION INDICES DEVELOPED FROM UNMANNED AERIAL SYSTEM DATA 16
Abstract 17
2.1 Introduction 18
2.2 Materials and Methods 19
2.3 Results and Discussion 26
2.3.1 Cloud Detection 26
2.3.2 Effect of Cloud Cover on Vegetation Indices 27
2.3.3 Effect of Cloud Cover on Reflectance 30

2.4 Conclusion 32
2.5 Acknowledgements 32
2.6 References 33
Chapter 3 - DIURNAL EFFECTS ON UNMANNED AERIAL VEHICLE-ACQUIRED SPECTRAL REFLECTANCE DATA IN COTTON AND SOYBEAN PRODUCTION 36
Abstract 37
3.1 Introduction 38
3.1.1 Potential Spatio-Temporal Factors 39
3.2 Materials and Methods 41
3.2.1 Image Acquisition 41
3.2.2 Image Analysis 45
3.3 Results and Discussion 45
3.4 Conclusions 52
3.5 Acknowledgements 52
3.6 References 53
Chapter 4 - IN-SEASON ASSESSMENT OF COTTON NITROGEN STATUS FROM A HANDHELD SMARTPHONE AND AN UNMANNED AERIAL SYSTEM 56
Abstract 57
4.1 Introduction 58
4.2 Materials and Methods 59
4.2.1 Ground-based Measurements 60
4.2.2 Aerial Measurements 62
4.2.3 Image Analysis 63
4.3 Results and Discussion 65
4.3.1 Ground-based Measurements 65
4.3.2 Aerial-based Measurements 68
4.3.3 Seed Cotton Yield 72
4.4 Conclusions 72
4.5 Acknowledgements 73
4.6 References 74

Chapter 5 – CONCLUSIONS AND USER RECOMMENDATIONS 78
5.1 Overview 79
5.2 Chapter 2 Conclusions 79
5.3 Chapter 3 Conclusions 80
5.4 Chapter 4 Conclusions 80
5.5 User Recommendations 81
5.6 Future Research 81
VITA 83

LIST OF TABLES

Table 1.1. Vegetation indices used in cotton production 9

Table 2.1. Spectral bands acquired by the MicaSense RedEdge camera 19

Table 2.2. Notation and description of the orthomosaic datasets used in this study. 22

Table 2.3. Vegetation indices used in this study, including normalized difference vegetation index (NDVI), green normalized difference vegetation index (GNDVI), and normalized difference red edge index (NDRE). 22

Table 2.4. Average vegetation indices (VIs) values for the whole field and cloudy subset for Fields 1 and 2. Means are compared pairwise within a VI and the whole field or cloudy subset assessment. Values not sharing a letter are significantly different by Fisher's protected least significant different (p≤0.05). 28

Table 2.5. Coefficient of variation (CV) for vegetation indices (VIs) for the whole field and cloudy subset for Fields 1 and 2. Mean CVs are compared pairwise within a VI and the whole field or cloudy subset assessment. Values not sharing a letter are significantly different by Fisher's protected least significant different (p≤0.05). 29

Table 2.6. Average reflectance values for the whole field and cloudy subset for Fields 1 and 2. Means are compared pairwise within a wavelength and the whole field or cloudy subset assessment. Values not sharing a letter are significantly different by Fisher's protected least significant different (p≤0.05). 31

Table 2.7. Average reflectance values for the whole field and cloudy subset for Fields 1 and 2. Means are compared pairwise within a wavelength and the whole field or cloudy subset assessment. Values not sharing a letter are significantly different by Fisher's protected least significant different (p≤0.05). 31

Table 3.1. Vegetation indices (VIs) and formulas used in this study 40

Table 3.2. MicaSense RedEdge camera specifications for band name, center wavelength (nm), and bandwidth (nm) 43

Table 3.3. Solar azimuth and elevation angles at each time of data acquisition 44

Table 3.4. Percentage non-vegetation (i.e. shadows and soil) present in each trial image at each time of data acquisition. Means were separated using Fischer's protected least significant difference test at P ≤ 0.05. *Soybean flight at 1200 h had a cloud covering most of the trial. 46

Table 3.5. Overall normalized difference vegetation index (NDVI) values for each flight time and crop trial. Means were separated using Fischer's protected least significant difference test at P ≤ 0.05. 47

Table 4.1. Treatments consisted of varied rates and timings of N; application A was made after emergence but prior to early square. Application B was made during the first week of flower. 61

Table 4.2. Planting, harvest, application, and data collection dates for each site-year. 61

Table 4.3. MicaSense RedEdge camera specifications for band name, center wavelength (nm), and bandwidth (nm) 63

Table 4.4. Selected vegetation indices (VIs) and corresponding references calculated within this study. 64

Table 4.5. Early-season (prior to 15 July) response of height, SPAD, DGCI, NDVI and leaf nitrogen (N) to applied fertilizer N rate averaged across site-year. Since measurements occurred prior to the second application timing, only data from the plots receiving all N fertilizer at the early application timing were included. 66

Table 4.6. Late-season response (After 15 July) of height, SPAD, DGCI, NDVI and leaf nitrogen (N) to applied fertilizer N rate and timing averaged across site-year. 67

Table 4.7. Pearson correlation (r) values between specified plant parameters, vegetation indices, and individual wavelengths from ground-based sensors and UAV-based sensors from 2016 Milan, 2017 Grand Junction (GJ), and 2017 Jackson prior to Application B. Significance levels are denoted by ** $p<0.01$ and * $p<0.05$. .. 70

Table 4.8. Analysis of variance (ANOVA) table for seed cotton yield response to site-year, replication nested within site-year, fertilizer nitrogen (N) rate, and fertilizer N timing. 72

LIST OF FIGURES

Figure 1.1. Bandwidth of selected spectral bands in MicaSense multispectral camera (MicaSense Inc., Seattle, WA).....3

Figure 1.2. Differences in multispectral and hyperspectral imaging (Mutanga et al., 2009). 5

Figure 2.1. Orthomosaic datasets used in this study include Field 1 with (a) partially cloudy conditions and (b) mostly sunny conditions and Field 2 with (c) partially cloudy conditions and (d) mostly sunny conditions. .21

Figure 2.2. Data is summarized at the plot scale seen here for (a) Field 1 and (b) Field 2 24

Figure 2.3. A subset of plots selected due to their cloudy condition in (a) Field 1, cloudy, (b) Field 2, cloudy, (c) Field 1, sunny, and (d) Field 2, sunny. 25

Figure 2.4. Brightness index (BI) map for (a) Field 1 and (b) Field 2 26

Figure 2.5. Brightness index values for clear and cloudy designated plots for Fields 1 and 2 27

Figure 3.1. Research trial plots in (a) cotton and (b) soybeans at the University of Tennessee West Tennessee Research and Education Center used in this study. Plot polygons represent the experimental unit. 42

Figure 3.2. Solar azimuth at each time (h) of data acquisition in the (a) cotton and (b) soybean trials 44

Figure 3.3. Variation in NDVI, NDRE, and SR throughout the day for each study treatment for the (a) cotton and (b) soybean trials 48

Figure 3.4. Reflectance values (%) in the blue (475 nm), green (560 nm), red (668 nm), red edge (717 nm), and near infrared (840 nm) wavelengths, separated by time of data acquisition for (a) the cotton trial and (b) the soybean trial. 49

Figure 3.5. Coefficient of variation (CV, %) for the overall datasets for cotton and soybeans in the blue (475 nm), green (560 nm), red (668 nm), red edge (717 nm), and near infrared (840 nm) wavelengths, as well as for NDVI 50

Figure 3.6. Coefficient of variation among flight times (0800, 1000, 1200, 1400, and 1600 h) at blue (475 nm), green (560 nm), red (668 nm), red edge (717 nm), and near infrared (840 nm) wavelengths for the (a) cotton and (b) soybean trials 51

Figure 4.1. Cotton nitrogen (N) trial orthomosaics from (left to right): Milan 2016, Jackson 2017, and Ames 2017 60

Figure 4.2. Relationships between leaf N and NDVI, DGCI, and SPAD graphed by sampling time, where the break between early and late is considered to be the second week of flower (typically 15 July). 67

Figure 4.3. Relationships between SPAD, DGCI, and NDVI across early and late sampling times. Data from the late season 2016-Grand Junction site-year was excluded due to the severe drought stress present prior to that sampling date. 69

Figure 4.4. A regression of SPAD measurements to ground-based or UAV-based DGCI predictions of chlorophyll as modeled by Wang et al. (2012). 71

Figure 4.5. Response of seed cotton yield to fertilizer nitrogen (N rate) graphed by site-year. Rates not sharing any letter are significantly different by the Fisher's protected least significant difference at the 5% level of significance. 73

CHAPTER 1 – INTRODUCTION

1.1 Background

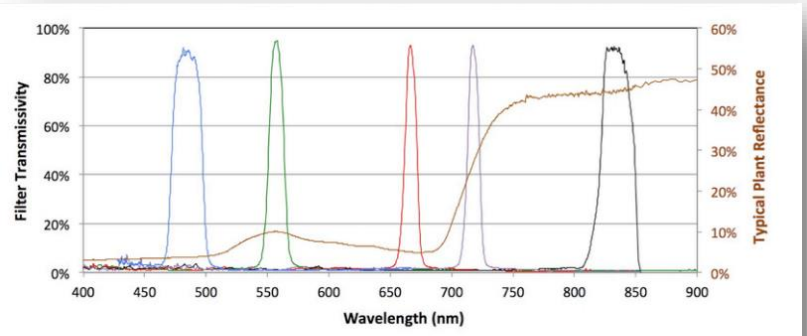
With increasing prices of nitrogen (N) fertilizers and the contribution of production agriculture to diminished water quality in the Mississippi River Basin (Alexander et al., 2008), nitrogen management practices need to be re-evaluated to better benefit producers and the environment. Best management practices that can increase nitrogen use efficiency will ultimately decrease the amount of nitrogen losses through leaching and runoff, which will lead to environmental and economic benefit. Nitrogen fertilizers have typically been applied uniformly across fields, regardless of the spatial variability within a field. Variable rate technology can be used to apply nitrogen fertilizer at the correct rate and in the correct place. Currently, there is a need for inexpensive methods that have the potential to be readily adopted to determine where and how much nitrogen fertilizer needs to be applied within a field.

1.1.1 In-Field Spatial Variability and Variable Rate Technologies

Variability exists in all crop production fields and can be attributed to factors such as soil physical and chemical properties, soil fertility, soil moisture, topography, pests and diseases (Zhang et al., 2002). Applying crop inputs on a site-specific basis in management zones—areas within a field that have a specific yield potential that respond to management practices in a similar way, instead of a uniform application based on the field average—has the potential to help producers maximize profitability and protect surface and ground water resources for crop production.

Variable rate technologies dispense or apply desired amounts of crop inputs such as seeds, pesticides and fertilizers in specific areas of an agricultural field in order to maximize productivity and decrease environmental impacts. There are several technologies commercially available to monitor and apply these production inputs based on the differentially-corrected Global Positioning System (GPS)/Global Navigation Satellite System (GNSS) location of farm equipment in the field and variable rate application maps. Variable rate application (VRA) of fertilizer applies the correct rate of nutrients in the correct location within a field. This technology has the potential to reduce nutrient inputs and increase nutrient use efficiency. In turn, the use of VRA may reduce the amount of nutrients that could ultimately pollute nearby streams, rivers and reservoirs.

One method of determining spatial variability is through remote sensing of crop reflectance. Remote sensing is a field of study that utilizes sensors to collect information about the amount of reflectance along the electromagnetic spectrum from a given object. In these studies, a MicaSense RedEdge multispectral camera (MicaSense Inc., Seattle, WA) was mounted to an unmanned aerial vehicle (UAV) for image acquisition. This camera has narrowband filters for blue, green, red, red-edge, and near-infrared spectral bands (Figure 1.1). There are numerous considerations when choosing a sensor such as the spatial, spectral, and radiometric resolution, as well as cost. These characteristics and sensor specifications are described in Section 1.2 Data Acquisition. In order to accurately quantify spatial variability within a crop, a vegetation index can be derived from remote imagery and then related to an application map. There are numerous vegetation indices that have been developed, but this research will evaluate the most common and/or those with the most potential of accurately defining spatial variability and relating this variability to a nitrogen application in order to optimize economic yield. These indices along with formulas are presented in Section 1.3 Vegetation Indices.



Band Number	Band Name	Center Wavelength (nm)	Bandwidth FWHM (nm)
1	Blue	475	20
2	Green	560	20
3	Red	668	10
4	Near IR	840	40
5	Red Edge	717	10

Figure 1.1. Bandwidth of selected spectral bands in MicaSense multispectral camera (MicaSense Inc., Seattle, WA).

1.2 Data Acquisition

1.2.1 Platforms

Remote sensed imagery has traditionally been captured via satellite, airplane, or ground-based systems. The use of satellites and planes to gather accurate data in a timely manner is difficult due to potential weather, cloud-cover, and personnel and access issues. Ground-based systems with real-time application capabilities have become increasingly popular, but most use the normalized difference vegetation index (NDVI) and are expensive due to high component costs. Other more recently developed platforms that are capable of rapidly acquiring imagery include smartphones and UAVs. The Pew Research Center (2019) reported that 81% of adults in the United States own a smartphone, up from 35% in 2011. These smartphones could potentially, and already have in some instances, replace other expensive ground-based measurement devices. A UAV is an unmanned aircraft that is controlled remotely or autonomously and that is capable of housing cameras and sensors such that the user can acquire geo-referenced imagery in a timely manner. With certain restrictions, UAVs have been integrated into the national airspace and are allowed to be used commercially. The largest sector expected to adopt this technology is agriculture for crop scouting, vegetation mapping, irrigation scheduling, and various other practices (AUVSI, 2013). As of September 2019, the United States Federal Aviation Administration (FAA) reported almost 1.5 million UAVs registered, with over 400k of those for commercial purposes, and over 153,000 UAV pilots certified (FAA, 2019).

1.2.2 Spatial Resolution

Spatial resolution refers to the smallest separation between two distinct objects that can be distinguished by a sensor (Jensen, 2007). In imagery, increasing spatial resolution translates to smaller pixel sizes. This parameter is dependent on the sensor's instantaneous field of view (IFOV), which is the angular region in which the sensor has visibility and the altitude of image acquisition. The pixel size is the product of the IFOV angle (in radians) and the altitude of the sensor (assuming the sensor is directly downward facing, or nadir). A narrower IFOV and/or images acquired at lower altitudes will result in smaller pixel sizes (i.e., higher spatial resolution). Typical spatial resolution for satellite imagery is between 10m and 1km, while aerial imagery collected from a UAV or airplane is typically <1cm to 1m. Relatively high spatial resolution is necessary for site-specific application of inputs in order to reduce background noise from non-

vegetation such as shadows and soil. Spatial resolution can be increased by (1) acquiring images from a lower altitude and/or (2) having a smaller sensor IFOV angle. Acquiring images at lower altitudes is feasible, but must be done while adhering to safety regulations or protocols. A smaller IFOV can cause a low signal-to-noise ratio because less energy and more background noise is being detected. There must be a balance between optimizing spatial and spectral resolution while maintaining a high signal-to-noise ratio.

1.2.3 Spectral Resolution

Spectral resolution is a function of the number of bands a sensor is capable of detecting and the width of those bands. A panchromatic sensor acquires images in 1 band, a multispectral sensor in 3-10 bands, and a hyperspectral sensor in >10 bands. Higher spectral resolution is represented by a narrower range of wavelengths for each band. Broader wavelength ranges can typically detect very distinct differences, while narrower ranges can detect subtler differences such as differences in crop vegetation. Figure 1.2 (Mutanga et al., 2009) is an example of reflectance readings from an extremely high resolution hyperspectral sensor and a lower resolution multispectral sensor. Note that the reflectance as measured by the hyperspectral sensor is represented by a continuous curve, while the multispectral readings are intermittent and represent a wider range of wavelengths.

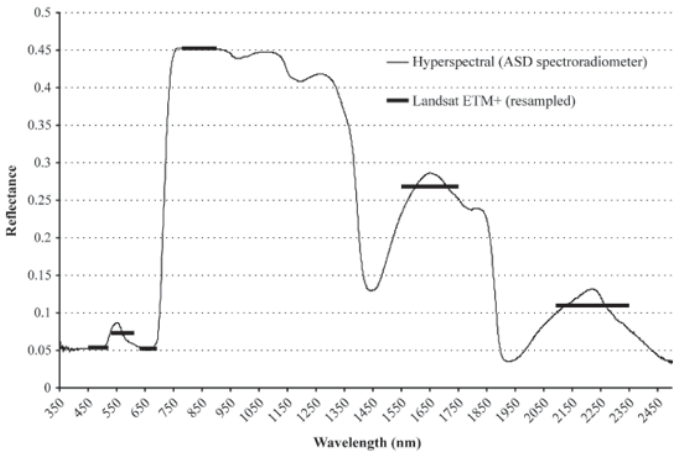


Fig. 1. Comparison between a hyperspectral (ASD FieldSpec 3 spectroradiometer; 2 150 bands, 350–2 500 nm) and the multi-spectral (Landsat ETM+) sensor. Landsat ETM+ bands are included as approximated from the ASD spectral input and do not represent the actual sensor response functions. The response in both cases represents a leaf-level sample from *Eucalyptus grandis*.

Figure 1.2. Differences in multispectral and hyperspectral imaging (Mutanga et al., 2009).

Hatfield and Pinter (1993) noted the need to detect small changes over a wide range of wavelengths to be able to determine differences in crop vigor. Spectral, radiometric, temporal, and spatial resolutions are not independent of one another, but can significantly affect each other. If the spectral resolution is increased by narrowing the wavelength band, less total energy and more background noise will be seen by the sensor (i.e. a low signal to noise ratio). The signal to noise ratio must be kept high to ensure image quality.

1.2.4 Radiometric Resolution

The radiometric sensitivity is defined by the ratio of the emitted to reflected electromagnetic energy. Each pixel in a radiometric image is represented by a digital number (DN). These digital numbers range from 0 to 2^n-1 where n represents the number of bits the sensor uses to represent the resolution of an image. For example, an 8-bit image will have DNs ranging from 0-255, while a 4-bit image will only have 16 DNs (0-15). Images with higher radiometric resolutions have more distinguishable detail than those with lower resolutions because there are more available bits of resolution to delineate one pixel from another. More detail can be obtained in an image by increasing the radiometric resolution of a sensor, but it also requires more memory.

1.2.5 Temporal Resolution

Temporal resolution describes the frequency at which imagery is acquired by a sensor. For satellites, this is a function of the satellites orbit. Aircraft, either manned or unmanned, can determine the frequency at which data is collected within the limits of weather and other external factors such as personnel availability. Time of day and crop phenological stage are also important temporal factors to consider in image acquisition. It is anecdotally recommended to fly within 2 hours of solar noon to avoid the sun casting shadows (Assmann et al., 2019). For in-season N application, image acquisition should occur near the time of application to determine the application rate – a knowledge of the crop growth pattern and N uptake capabilities is necessary. Many applications only require one image, but there are also many more that would benefit from multiple images of the same area of interest taken at a certain frequency. For example, images of a crop could be acquired weekly during a growing season to track crop health, pest pressure, etc. Disadvantages of increasing temporal resolution for aerial-acquired images include weather and time constraints, memory storage, and available personnel.

1.2.6 Optimization of Resolutions

For the purpose of agricultural applications, certain resolutions are worth the cost and difficulty to increase them. The optimal spatial resolution of unmanned aerial acquired imagery is 1-3cm. Although N cannot be applied at that resolution, it allows us to detect shade from individual leaves, potentially spot insects and diseases, etc. Ideally, a camera would have a spectral resolution of at least five bands (R, G, B, RedEdge, NIR) with relatively narrow bandwidth (more than a hacked digital camera, less than a hyperspectral sensor). Radiometric resolution should be at least 8-bit, with higher resolution improving the ability to distinguish small objects (Alonso et al., 2017; Jensen, 2007). Temporal resolution completely depends on the research question – some targets need to be flown only once while others need to be flown periodically throughout the growing season to evaluate changes over time. There are trade-offs to any increase in resolution that need to be evaluated thoroughly.

1.2.7 Calibration

Without calibration, imagery taken at different times or dates cannot be compared. Those reflectance values would just be relative to one another. If images are calibrated to negate specific environmental conditions at the time of image acquisition, we are able to better compare these images over time.

The most common radiometric calibration methods include the use of a broad spectrum reference panel. Reference materials with near-Lambertian reflectance properties can be imaged before and after, or even during, a flight. These materials have known reflectance properties across the electromagnetic spectrum. These often accompany newer sensors and have been tested to determine the reflectance of the specific spectrum of the corresponding sensor. There are several known standard reflectance panels with specifications along the entire electromagnetic spectrum. The most popular reference panel has the top flat surface made from barium sulfate, which is white in the visible spectrum but also has NIR features. Data can be calibrated to the in-field image of these reference materials through a simple calibration using the known reflectance of the reference panel along with an image of the reference panel taken in field. This method is fairly straightforward and accurate if the reflectance properties of the reference panel have been previously determined for the specific sensor being used (Hruska et al., 2012). It is relatively inexpensive and is one of the more popular methods of calibration in the industry (MicaSense Inc., Seattle, WA).

Either an on-board or ground-based spectroradiometer that is facing directly upwards can be used to measure incoming radiation across the same spectrum as the sensor. An on-board spectroradiometer can account for mid-flight changes in conditions, such as intermittent clouds. Images can then be normalized to the amount of incoming radiation at specific wavelengths to be able to better compare datasets over time.

1.3 Vegetation Indices

While crop reflectance data alone can provide some information on spatial variability of a crop, a vegetation index (VI) map can be developed from reflectance data to better highlight and emphasize this spatial variability. While there are numerous VIs in the literature, those that have shown the most promise for row crop production are listed in Table 1.1 and described herein.

The most common commercially-used vegetation index is the normalized difference vegetation index, or NDVI. Recently, research has shown that NDVI correlates poorly with cotton leaf N status (Raper et al., 2013; Raper and Varco, 2015) and many are beginning to question the accuracy of NDVI maps produced from high resolution aerial images due to variability in light conditions. The simple ratio (SR) and the modified soil adjusted vegetation index ($MSAVI_2$) were developed during the time that satellite remote sensing was becoming more available and popular. The SR is one of the first VIs in the literature (Jordan, 1969) and was created in order to be an indirect measurement of leaf area index. The $MSAVI_2$ is a simpler version of the original soil adjusted vegetation index (SAVI) and the modified soil adjusted vegetation index (MSAVI), but all of these attempt to account for soil background using a soil adjustment factor. The most promising vegetation indices for estimation of crop nitrogen status are those that use information from the red edge spectral band, such as the normalized difference red edge vegetation index (NDRE) and the simplified canopy chlorophyll content index (SCCCI). Raper and Varco (2015) determined that the red edge wavelength and red-edge based VIs were most closely correlated with mid-season leaf N in cotton.

All of the aforementioned VIs utilize reflectance from the non-visible regions and would require relatively expensive instruments due to the need for a multispectral sensor. Karcher and Richardson (2003) found that hue, saturation, and brightness (HSB) levels could be used to explain nitrogen status in turfgrass plots

Table 1.1. Vegetation indices used in cotton production

Vegetation Index	Full Name	Formula	Reference
NDVI	Normalized difference vegetation index	$\frac{R_{NIR} - R_{Red}}{R_{NIR} + R_{Red}}$	Rouse et al., 1973
GNDVI	Green normalized difference vegetation index	$\frac{R_{NIR} - R_{Green}}{R_{NIR} + R_{Green}}$	Gitelson et al., 1996
NDRE	Normalized difference red edge index	$\frac{R_{NIR} - R_{Red\,Edge}}{R_{NIR} + R_{Red\,Edge}}$	Gitelson and Merzlyak, 1994
DGCI	Dark green color index	$\frac{\left[\frac{Hue - 60}{60} + (1 - Saturation) + (1 - Brightness)\right]}{3}$	Karcher and Richardson, 2003
SCCCI	Simplified canopy chlorophyll content index	$\frac{NDRE}{NDVI}$	Barnes et al., 2000
MSAVI$_2$	Modified soil adjusted vegetation index	$\frac{1}{2}\left[2 * R_{NIR} + 1 - \sqrt{(2 * R_{NIR} + 1)^2 - 8(R_{NIR} - R_{Red})}\right]$	Qi et al., 1994
SR	Simple ratio	$\frac{R_{NIR}}{R_{Red}}$	Jordan, 1969

using a regular digital camera and developed the dark green color index (DGCI) based on those HSB levels; Raper et al. (2012) further evaluated the use of DGCI in cotton and found positive correlations between DGCI and leaf chlorophyll measurements. A more inexpensive camera with acceptable accuracy in estimating plant N status and good separation of spatial variability would be beneficial in progressing the adoption of remote sensing in cotton production.

1.3.1 Applications

The ultimate goal of measuring reflectance and developing vegetation index maps is to improve management decisions, generally of fertilizer inputs. Algorithms have been developed in some commercial systems such as GreenSeeker (Trimble Inc., Sunnyvale, CA) to relate a vegetation index value to a nitrogen (N) application rate such that the N rate can be varied spatially throughout the field. These algorithms are generally developed with N rate trials in the crop of interest; a sensor is used to acquire the spectral reflectance, a vegetation index is derived, and these are correlated with yield and N application rate.

1.4 Potential UAV Data Quality and Stability Issues

The use of unmanned aerial systems (UASs) in agriculture has markedly increased since their legal inclusion into the United Spaces airspace. Producers, consultants, and advisors are using UASs to quickly assess a crop field and are making management decisions based on this assessment. Due to low cost and accessibility, many companies and individuals are employing UASs without any training or background in remote sensing. Furthermore, these users often operate the UAS at the most convenient time which may or may not fall near solar noon, a period in which shadows are reduced and conditions within the field of view are fairly consistent. Operating with disregard to standard remote sensing data collection guidelines can damage data quality and stability.

Two of the main environmental effects on data soundness include cloud cover and time of day of data acquisition. Transient cloud cover is typical in humid areas during the growing season when UAV flights occur. These clouds can induce shading of portions of a canopy and can move during image acquisition, potentially causing data quality as well as image processing issues. The time of day of UAV flight and data acquisition could also have an effect on the data quality due to several spatio-temporal factors: the

changing solar angle of incidence, heliotropic movement of certain agronomic crops, flight pattern of the UAV, and the presence of dew on the crop. Vegetation indices (VIs) are calculated based on measures of crop reflectance and are therefore potentially vulnerable to diurnal and cloud cover effects. Both cloud cover and time of day pose a logistical challenge for UAV users, as the typical UAV user may not be willing or able to wait for ideal conditions.

Current instruments to measure crop reflectance are costly and time consuming. With the decreasing price of smartphones and UAVs, these platforms could provide a rapid and effective method of developing VI maps to be used to inform agronomic management decisions. Essential to the success and adoption of these platforms is the development of VIs using reflectance within the visible range so as to further reduce the price and simplicity of the system. Additionally, VIs derived from UAV-based data may not be directly comparable or interpreted the same as VIs from ground-based data due to scale.

1.5 Objectives

The overarching objective of this dissertation is to ensure data quality and to enhance the utility of information collected by unmanned aerial systems (UASs) in agricultural crop production systems. Specifically, the objectives are to:

1. Identify environmental attributes that impact the stability of vegetation index (VI) maps derived from UAS-acquired data and develop recommendations for standard operating procedures
    a. Determine how shading from cloud cover affects VI maps. [Chapter 2]
    b. Determine if time of day of data acquisition affects VI maps. [Chapter 3]
2. Identify image acquisition and post-processing techniques to enhance the utility of VI maps derived from smartphone and UAS-acquired data [Chapter 4]

1.5.1 Dissertation Composition

This dissertation consists of a general introduction, three manuscripts, and a concluding chapter:

1. Chapter 1: An introduction to the concepts and ideas presented in the manuscripts. This Chapter includes stated dissertation objectives and composition.
2. Chapter 2: This manuscript investigates the effect of shading from transient cloud cover on vegetation indices (VIs) in agricultural crop production with UAV-collected data. This manuscript

has planned submission to the journal Remote Sensing in the Environment. The manuscript addresses:

   a. The effect of cloud cover on VIs
   b. The effect of cloud cover on reflectance values in individual bands
   c. Recommendations to users regarding data acquisition
   d. A proposed solution to the potential issue of cloud cover

3. Chapter 3: This manuscript examines the influence that the time of day of UAV-data acquisition has on vegetation indices (VIs). This manuscript has planned submission to the journal Remote Sensing in the Environment. The manuscript addresses:
   a. The effect time of day of data acquisition from a UAV has on VIs
   b. The effect time of day of data acquisition from a UAV has on reflectance values in individual bands
   c. Recommendations to users regarding data acquisition
4. Chapter 4: This manuscript analyzes UAV and ground-based data to estimate plant nitrogen (N) status in a cotton crop as a substitute for more expensive and time consuming technologies. This manuscript has planned submission to the Journal of Cotton Science. The manuscript addresses:
   a. Smartphone and UAV measurements to estimate cotton N status
   b. Correlations to current measurement technologies (SPAD)
   c. Comparison of ground- to UAV-based measurements
5. Chapter 5: This chapter contains conclusions, recommendations, and areas for future work.

1.6 References

Alexander, R. B., R. A. Smith, G. E. Schwarz, E. W. Boyer, J. V. Nolan, and J. W. Brakebill. 2008. Differences in phosphorus and nitrogen delivery to the Gulf of Mexico from the Mississippi River Basin. *Environ. Sci. Technol.* 42(3): 822-830.

Alonso, C., A. Tarquis, I. Zuniga, and R. Benito. 2017. Spatial and radiometric characterization of multi-spectrum satellite images through multi-fractal analysis. Nonlinear Processes in Geophysics 24: 141-155.

Assmann, J., J. Kerby, A. Cunliffe, and I. Myers-Smith. 2019. Vegetation monitoring using multispectral sensors – best practices and lessons learned from high latitudes. Journal of Unmanned Vehicle Systems 7(1): 54-75.

AUVSI. 2013. The economic impact of unmanned aircraft systems integration in the United States. Association for Unmanned Vehicle Systems International.

Barnes, E., T. Clarke, S. Richards, P. Colaizzi, J. Haberland, M. Kostrzewski, P. Waller, C. Choi, E. Riley, T. Thompson, R. Lascano, H. Li, and M. Moran. 2000. Coincident detection of crop water stress, nitrogen status, and canopy density using ground based multispectral data. Unpaginated CD-ROM (13.pdf). *In* Proceedings of the 5th International Conference on Precision Agriculture, Bloomington, MN 16–19 July 2000. ASA, CSSA, and SSSA, Madison, WI.

FAA. 2019. "UAS by the numbers." *Federal Aviation Administration.* 7 October 2019, https://www.faa.gov/uas/resources/by_the_numbers/.

Gitelson, A. and M. Merzlyak. 1994. Quantitative estimation of chlorophyll using reflectance spectra. Journal of Photochemistry and Photobiology B: Biology 22: 247–252.

Gitelson, A.A., Y.J. Kaufman, and M.N. Merzlyak, 1996. Use of a green channel in remote sensing of global vegetation from EOS-MODIS. *Remote Sens. Environ.,* 58: 289-298.

Hatfield, J. and P. Pinter. 1993. Remote sensing for crop protection. Crop Protection 12(6): 403-413.

Hruska, R., J. Mitchell, M. Anderson, and N. Glenn. 2012. Radiometric and geometric analysis of hyperspectral imagery acquired from an unmanned aerial vehicle. Remote Sens. 4: 2736-2752.

Jensen, J. 2007. *Remote Sensing of the Environment* (2nd edition). Pearson Prentice Hall.

Jordan, C. 1969. Derivation of leaf-area index from quality of light on the forest floor. Ecology 50(4): 663-666.

Karcher, D. and M. Richardson. 2003. Quantifying turfgrass color using digital image analysis. Crop Sci. 43: 943-951.

Mutanga, O., J. van Aardt, and L. Kumar. 2009. Imaging spectroscopy (hyperspectral remote sensing) in southern Africa: an overview. South African Journal of Science 105: 5-6.

Pew Research Center. 2019. "Mobile Fact Sheet." *Pew Research Center, Internet and Technology*. 7 October 2019, https://www.pewinternet.org/fact-sheet/mobile/.

Qi, J., A. Chehbouni, A. Huete, Y. Kerr, and S. Sorooshian. 1994. A modified soil adjusted vegetation index. Remote Sens. Environ. 48: 119-126.

Raper, T., D. Oosterhuis, U. Siddons, L. Purcell, and M. Mozaffari. 2012. Effectiveness of the dark green color index in determining cotton nitrogen status from multiple camera angles. International Journal of Applied Science and Technology 2(1): 71-74.

Raper, T. B., J. J. Varco, and K. J. Hubbard. 2013. Canopy-based normalized difference vegetation index sensors for monitoring cotton nitrogen status. Agron. J. 105: 1345-1354.

Raper, T. and J. Varco. 2015. Canopy-scale wavelength and vegetative index sensitivities to cotton growth parameters and nitrogen status. Precision Agriculture. 16(1): 62-76.

Rouse, J., R. Haas, J. Schell, and D. Deering. 1973. Monitoring vegetation systems in the Great Plains with ERTS. p. 9-317. Third Earth Resources Technology Satellite-1 Symposium. NASA Sp-351 I, Greenbelt, MD.

Zhang, N., M. Wang, and N. Wang. 2002. Precision agriculture – a worldwide overview. Computers and Electronics in Agriculture 36: 113-132.

CHAPTER 2 - EFFECT OF CLOUD COVER ON VEGETATION INDICES DEVELOPED FROM UNMANNED AERIAL SYSTEM DATA

Abstract

Unmanned aerial systems (UAS) are increasingly being used in production agriculture to acquire aerial imagery in a time- and cost-effective manner to make in-season management decisions. Many crop advisors and producers will use multispectral data to compute a vegetation index (VI), such as the normalized difference vegetation index (NDVI), to assess crop health and to make management decisions on a spatial basis. Atmospheric and radiometric calibrations are normally applied to UAS-acquired data. However, intermittent and fast-moving clouds are often present, potentially introducing variability in reflectance data. This study used UAS-acquired imagery of two soybean fields in both sunny and cloudy conditions in order to make comparisons of VIs and reflectance data. Reflectance parameters included blue (475 nm); green (560 nm); red (668 nm); red edge (717 nm); and near infrared (840 nm). Vegetation indices included NDVI; green normalized difference vegetation index (GNDVI); normalized difference red edge index (NDRE); modified soil adjusted vegetation index 2 (MSAVI2); and simple ratio (SR). Analysis revealed that shadows cast by clouds can have a significant effect on normalized difference VIs ($p \leq 0.05$), however these differences are not great enough to warrant a management change. However, with both datasets used in this analysis, the reflectance in individual bands is consistently and significantly affected by cloud cover ($p \leq 0.05$). This has implications for other VIs such as MSAVI2, or for other uses of reflectance data.

Keywords: UAV, UAS, agriculture, NDVI, vegetation index, clouds, shadows

2.1 Introduction

The use of unmanned aerial vehicles (UAVs) in production agriculture has increased significantly (AUVSI, 2013) in the last several years, but little guidance in standard operating procedures are available to the novice user. Many producers and industry professionals are adopting the technology without knowledge around data collection, management, analysis, and how to translate information into management decisions. One common application in the field of precision agriculture is the use of vegetation indices (VIs) such as the normalized difference vegetation index (NDVI) to monitor a crop and to guide management decisions. NDVI is calculated based on measures of crop reflectance and is therefore vulnerable to the potential effects of cloud cover. Cloud cover poses a logistical challenge for UAV users, as it is constantly changing and the typical UAV user may not wait for ideal data collection conditions. This study aims to evaluate the effect of shadows from cloud cover on commonly used VIs, such as NDVI.

For mapping purposes in row crop agriculture, a flight pattern is typically programmed into the UAV autopilot such that the UAV automatically flies and captures imagery at predetermined locations. Depending on the desired spatial resolution and flight altitude, several hundred images may be acquired for a small field. Image processing software is then used to stitch overlapping images into an orthomosaic, or one single image, using statistical analyses. The orthomosaic is then used to calculate VIs that the user can consider when making management decisions.

Some multispectral cameras (those collecting reflectance data between three and ten bands) currently on the market have integrated upward-dwelling irradiometers to be triggered with every individual image acquired of the field such that site- and time-specific atmospheric calibrations can be conducted. However, manufacturers admit that even this level of calibration does not function well with intermittent, fast moving clouds. Additionally, geometric characteristics complicate this method of calibration. The changing position of the UAV, cloud position, irradiometer angle, sensor angle, and sun angle can all impact the final reflectance value. Advanced algorithms exist that can automatically detect and correct for shadows (Adeline et al., 2013; Gong and Cosker, 2017; Simic Milas et al., 2017), but, to the authors' knowledge, these algorithms are not integrated into the common UAV data processing software packages. A novice user, especially without best practice guidance, is not likely to seek out these algorithms.

The main objective of this study was to determine if cloud cover significantly affects vegetation indices (VIs) or reflectance in the individual bands acquired from a UAV. If so, standard operating procedures may be developed to minimize these errors resulting from images with partial cloud cover.

2.2 Materials and Methods

A custom quadcopter UAV equipped with a MicaSense RedEdge multispectral camera (MicaSense Inc., Seattle, WA) was used to collect aerial imagery of two fields containing small-plot research at the University of Tennessee Milan Research and Education Center (35°56'04.7"N 88°43'40.2"W) on 26 July 2016 and 9 September 2016. Research trials, though not evaluated in this study, were designed to evaluate the response of several soybean cultivars to varying fungicide timings, rates, and products. The UAV flew a programmed mission at a speed of 17.6 km hr^{-1} and an altitude of 30 m above ground level, resulting in a spatial resolution of 1.9 cm. The multispectral camera captured one image per second in five narrow bands, described in Table 2.1. Bandwidth is defined as the width of the transmissivity curve at half of the peak transmissivity, or full width at half maximum (FWHM).

Table 2.1. Spectral bands acquired by the MicaSense RedEdge camera

BAND	CENTER WAVELENGTH (nm)	BANDWIDTH (nm) at full width at half maximum (FWHM)
Blue	475	20
Green	560	20
Red	668	10
Red Edge	717	10
Near Infrared	840	40

Field 1 data (Figures 2.1a and 2.1b) was collected on 9 September 2016 as soybeans were reaching maturity (100 days after planting, DAP) and Field 2 data (Figures 2.1c and 2.1d) was collected 26 July 2016 (55 DAP). Data was collected twice using the same flight pattern within half an hour to represent conditions that were visually perceived to be cloudy (Figures 2.1a and 2.1c) and sunny (Figures 2.1b and 2.1d). Orthomosaics were generated by the Atlas (MicaSense Inc., Seattle, WA) cloud-based service and downloaded as a 16-bit GeoTIFF file. These orthomosaics are denoted as Field 1-cloudy, Field 1-sunny, Field 2-cloudy, and Field 2-sunny in the remainder of this report and are further described in Table 2.2. Image processing described herein was performed in ArcMap 10.5 (ESRI, Redland, CA).

The normalized difference vegetation index (NDVI), green normalized difference vegetation index (GNDVI), normalized difference red edge index (NDRE), modified soil adjusted vegetation index (MSAVI2), and the simple ratio (SR) were calculated for each dataset (Table 2.3). These VIs were calculated for all images on the original orthomosaic datasets spatial resolution of 1.9 cm.

Orthomosaic images were compared in order to analyze the effect of cloud cover on VIs. A typical analysis of high resolution data would use spatial alignment to compare and contrast multiple images. Change detection algorithms are well documented in the literature (Lu et al., 2004; Minu and Shetty, 2015; Radke et al., 2005). These algorithms are intended to look at change in multi-temporal datasets, historically for low-resolution satellite imagery. Perhaps the most important parameter for accurate use of change detection algorithms is spatial image registration (Lu et al., 2004). Although UAVs can provide high spatial resolution, most use the global position system (GPS) with wide area augmentation system (WAAS) differential correction resulting in horizontal accuracies of approximately 3 m. This results in images that do not align spatially, even with ground control points and the use of rectification in a GIS (geographic information system) software. This study reduces the spatial resolution of the dataset to be able to compare known areas in the field between the two images and to better align with the spatial resolution at which agricultural fertilizers and chemicals can realistically be applied.

Agricultural fertilizer or chemical applications that are made based off of remotely sensed imagery are generally performed at a scale of approximately 5 m and over a 5-second time frame (moving at 16 km hr^{-1} = 22 m) (Taylor and Fulton, 2010). When using imagery to relate to an application, extremely high

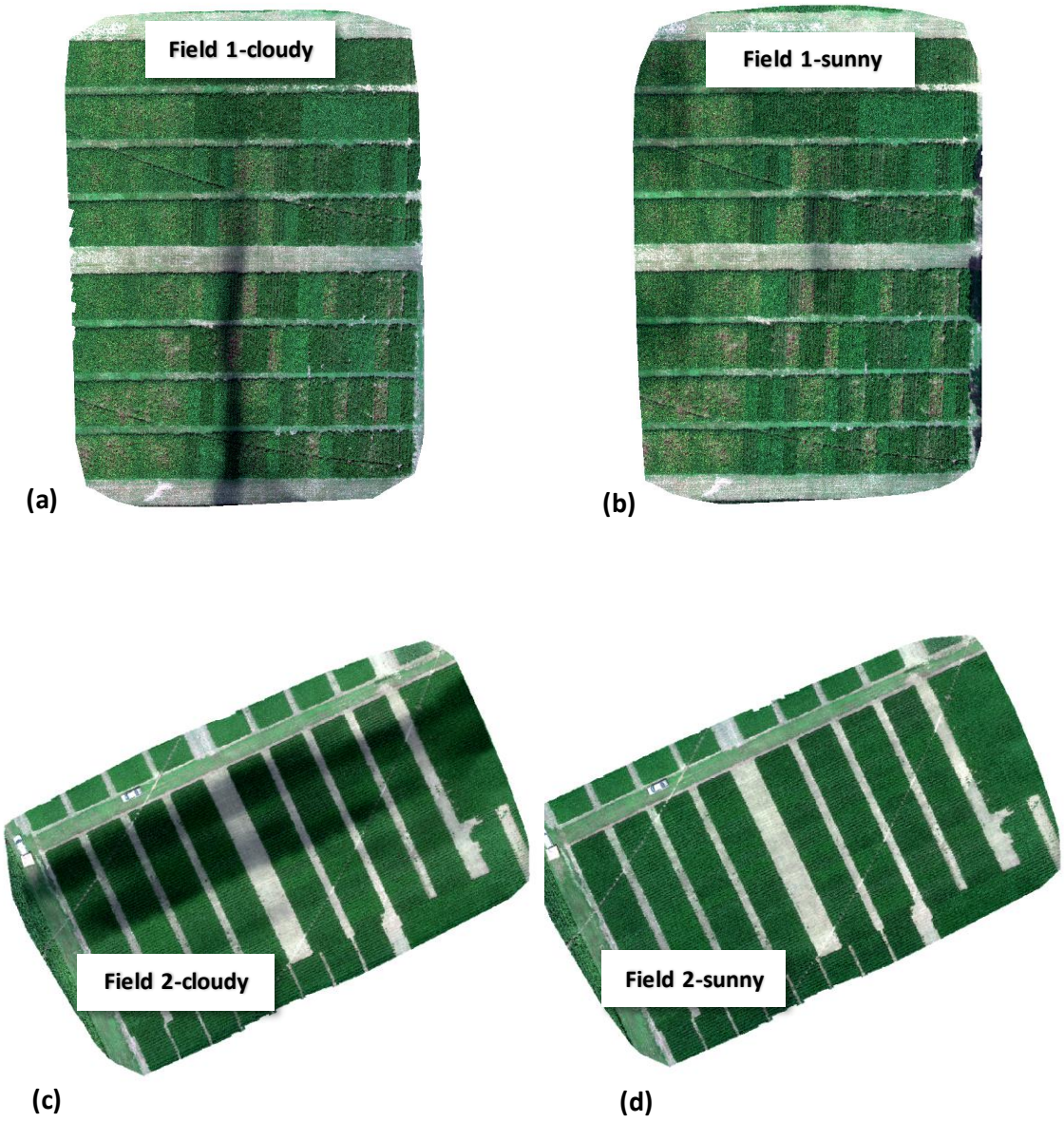


Figure 2.1. Orthomosaic datasets used in this study include Field 1 with (a) partially cloudy conditions and (b) mostly sunny conditions and Field 2 with (c) partially cloudy conditions and (d) mostly sunny conditions.

Table 2.2. Notation and description of the orthomosaic datasets used in this study.

Notation	Description
Field 1-cloudy	Field 1, partially cloudy in middle of field (Figure 2.1a)
Field 1-sunny	Field 1, mostly sunny (Figure 2.1b)
Field 2-cloudy	Field 2, partially cloudy in northern part of field(Figure 2.1c)
Field 2-sunny	Field 2, mostly sunny (Figure 2.1d)

Table 2.3. Vegetation indices used in this study, including normalized difference vegetation index (NDVI), green normalized difference vegetation index (GNDVI), and normalized difference red edge index (NDRE).

Vegetation Index	Full Name	Formula	Reference
NDVI	Normalized difference vegetation index	$\frac{R_{NIR} - R_{Red}}{R_{NIR} + R_{Red}}$	Rouse et al., 1973
GNDVI	Green normalized difference vegetation index	$\frac{R_{NIR} - R_{Green}}{R_{NIR} + R_{Green}}$	Gitelson et al., 1996
NDRE	Normalized difference red edge index	$\frac{R_{NIR} - R_{Red\,Edge}}{R_{NIR} + R_{Red\,Edge}}$	Gitelson and Merzlyak, 1994
$MSAVI_2$	Modified soil adjusted vegetation index	$\frac{1}{2}\left[2 * R_{NIR} + 1 - \sqrt{(2 * R_{NIR} + 1)^2 - 8(R_{NIR} - R_{Red})}\right]$	Qi et al., 1994
SR	Simple ratio	$\frac{R_{NIR}}{R_{Red}}$	Jordan, 1969

resolution data is unnecessary and increases processing time. Due to the original orthomosaics having extremely high spatial resolution (3.6 cm^2) and the need to compare two images that did not spatially align at that scale, each orthomosaic was subdivided into treatment plots that were 4 rows wide (approximately 3 m) by 9 m in length (Figure 2.2). Descriptive statistics of the calculated VIs as well as reflectance in individual bands (R, G, B, Red Edge, and NIR) were summarized by plot and the mean and standard deviation was assigned at the plot scale.

Each plot was manually assigned a cloudy or clear designation by visual inspection. Another less subjective method was also developed, using brightness as the indicator for presence of a cloud. Brightness was calculated as the average of reflectance in the red (668 nm), green (560 nm), and blue (475 nm) wavelengths (Bajwa and Tian, 2002). A brightness index (BI) was developed as the ratio of brightness in the cloudy image to the brightness in a sunny image of the same field, as shown in Equation 2.1.

Equation 2.1. Brightness index (BI) for cloud delineation between two images

$$BI = \left(\frac{Brightness_{cloudy\,image}}{Brightness_{sunny\,image}}\right) * 100$$

Due to concern that the whole image assessments could be diluted due to the high proportion of sunny to cloudy plots, a subset of the plots that contained clouds in only one image were also analyzed (Figure 2.3). Whole image assessments analyzed all plots in the images, while subset assessments analyzed the selected cloudy plots and the coinciding sunny plots in the other datasets. Plot data were subjected to analysis of variance in SAS (v9.5, SAS Institute, Cary, NC) to test for significance and means were separated using Fischer's protected least significant difference test at $P \leq 0.05$.

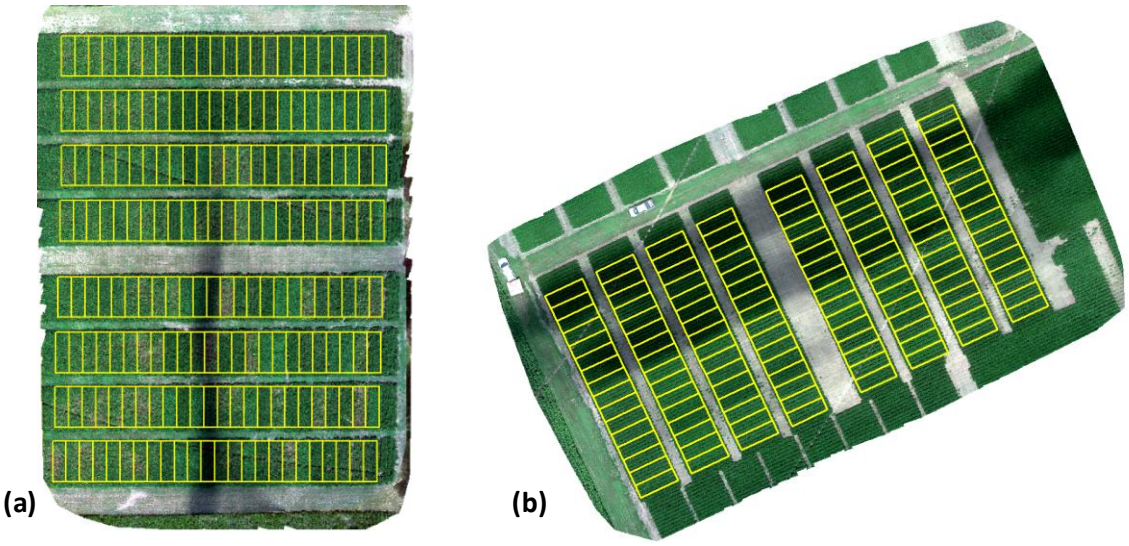


Figure 2.2. Data is summarized at the plot scale seen here for (a) Field 1 and (b) Field 2

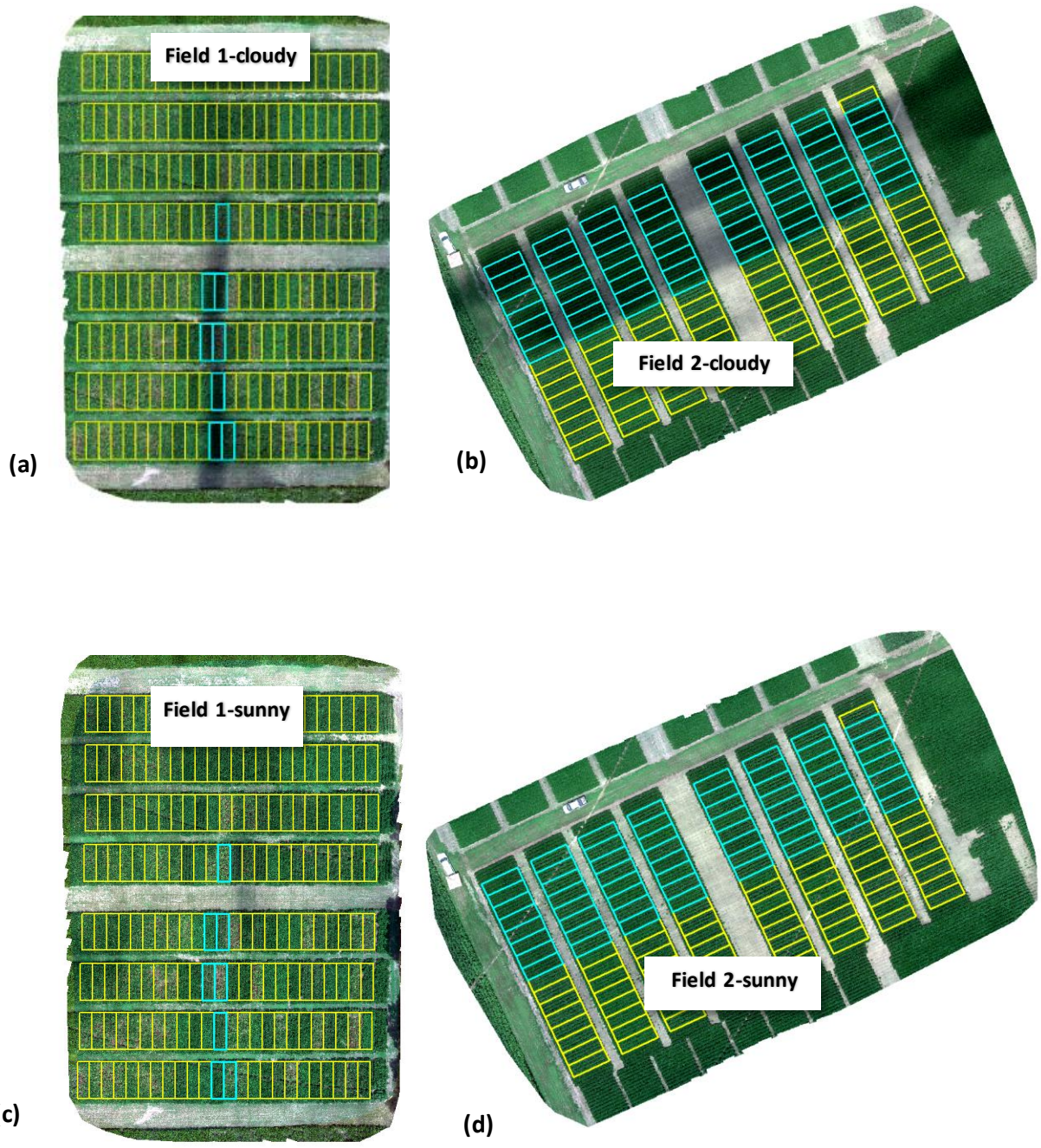


Figure 2.3. A subset of plots selected due to their cloudy condition in (a) Field 1, cloudy, (b) Field 2, cloudy, (c) Field 1, sunny, and (d) Field 2, sunny.

2.3 Results and Discussion

2.3.1 Cloud Detection

The brightness index appeared to successfully delineate clouds in both fields (Figure 2.4), even showing variability in shading that can occur with clouds with different opacities (Bajwa and Tian, 2002). Figure 2.5 displays BI averages and standard deviations of plots that had been manually designated as cloudy or clear for both fields. Note that the clear plots are at or above 100%, indicating similarity in both the sunny and cloudy images. Cloudy plots in both fields had an average BI around 50%, supporting the manual designations made for the analysis. This method and index could potentially be automated and used in post-processing UAV data where clouds present an issue.

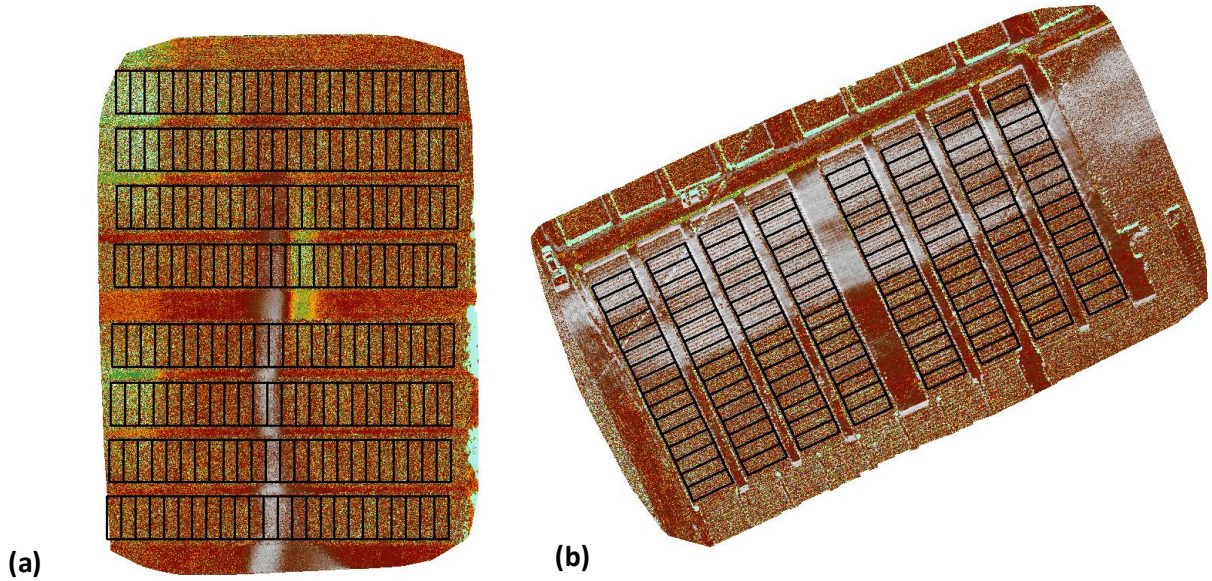


Figure 2.4. Brightness index (BI) map for (a) Field 1 and (b) Field 2

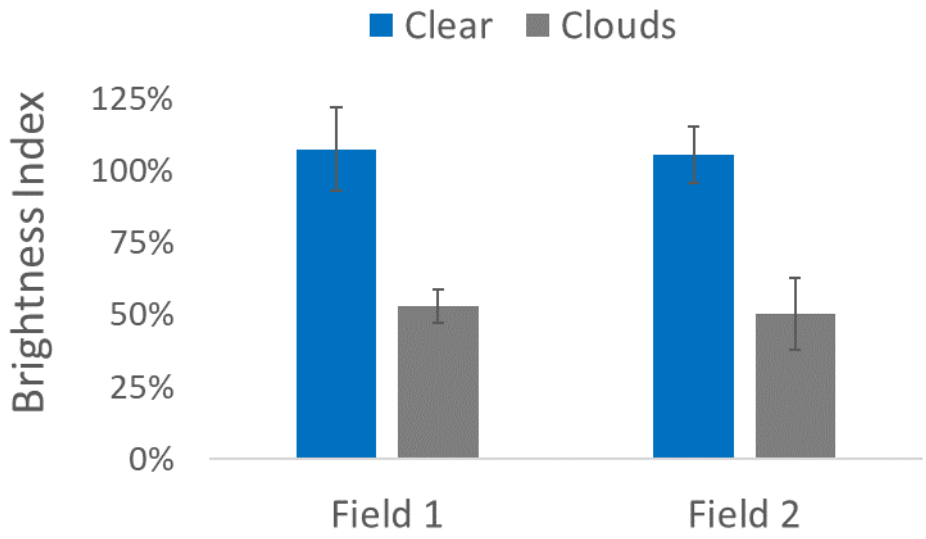


Figure 2.5. Brightness index values for clear and cloudy designated plots for Fields 1 and 2

2.3.2 Effect of Cloud Cover on Vegetation Indices

Average VI values for each plot are compared for the entire fields in Table 2.4. Field 1 had no significant differences in any VI between the cloudy and sunny images. This can be attributed to a high proportion of the field having no cloud cover, as only a small cloud was present. The subset analysis for Field 1 was largely similar to the whole field analysis, except for the differences seen in MSAVI2. Field 2 had a much larger area in cloud cover than Field 1, thus the whole field assessment did have statistically significant differences in NDVI, GNDVI, MSAVI2, and SR mean index values. Furthermore, the subset analysis reflected similar findings to the whole field analysis with every VI displaying a significant difference besides NDRE. Although significant, only small differences were seen in NDVI and GNDVI, followed by a moderate difference in SR, and a large difference in MSAVI2, which increased when only observing the cloudy subset. These differences were also observed by Zhang et al. (2015) when analyzing VI sensitivity to shadows. It should be noted that the minute differences in NDVI and GNDVI would not realistically translate into different management decisions due to the noise associated with measurements as witnessed by low coefficients of determination with corn leaf N in Yin and McClure (2013) and insensitivity to plant nitrogen status in cotton (Raper and Varco, 2015; Raper et al., 2013; Bronson et al., 2005). From relationships in the literature, an estimated 10 kg/ha increase in N uptake would increase NDVI from 0.7

to 0.75 for wheat (Lukina et al., 2001), sorghum (Moges et al., 2007), and corn (Xia et al., 2016), after which point the response begins to plateau.

Within plot variation of VIs is represented by coefficient of variation (CV) values in Table 2.5. Field 1 had several plots that were partially shaded so the comparison of all plots in the image would inherently have more within-plot variation. There was less within-plot variation in the Field 1 subset as noted by the similar CVs in Table 2.5, due to any partially shaded plots being excluded from the subset analysis. Field 2 had more cloud cover over the entire field, thus the within-plot variation for the whole field was somewhat similar to the subset analysis. There were significant ($P \leq 0.05$) differences in the CV in NDRE in Fields 1 and 2, as well as for GNDVI in Field 1 and MSAVI2 in Field 2. Zhang et al. (2015) also found a wider range in NDRE and MSAVI2 in images that were partially sunlit and partially shaded, as compared to NDVI. Plant reflectance in the red edge band (717 nm) is higher than the in the visible range and has more variability as seen in the CV of NDRE in Field 1 and Field 2. These findings infer that there are potential differences in the individual bands that are used to calculate the VIs. In addition, these results suggest that MSAVI2 is more sensitive to cloud cover than the other normalized difference VIs.

Table 2.4. Average vegetation indices (VIs) values for the whole field and cloudy subset for Fields 1 and 2. Means are compared pairwise within a VI and the whole field or cloudy subset assessment. Values not sharing a letter are significantly different by Fisher's protected least significant different ($p \leq 0.05$).

	WHOLE FIELD		CLOUDY SUBSET	
	Field 1-1 (cloudy)	**Field 1-2 (sunny)**	**Field 1-1 (cloudy)**	**Field 1-2 (sunny)**
NDVI	0.857 a	0.853 a	0.837 a	0.822 a
GNDVI	0.757 a	0.764 a	0.718 a	0.745 a
NDRE	0.456 a	0.464 a	0.439 a	0.442 a
MSAVI2	0.697 a	0.708 a	0.400 b	0.672 a
SR	16.5 a	15.9 a	15.1 a	13.5 a
	Field 2-1 (cloudy)	**Field 2-2 (sunny)**	**Field 2-1 (cloudy)**	**Field 2-2 (sunny)**
NDVI	0.934 a	0.929 b	0.935 a	0.930 b
GNDVI	0.835 b	0.845 a	0.826 b	0.846 a
NDRE	0.587 a	0.589 a	0.586 a	0.590 a
MSAVI2	0.664 b	0.848 a	0.484 b	0.852 a
SR	33.3 a	31.2 b	33.9 a	31.4 b

Table 2.5. Coefficient of variation (CV) for vegetation indices (VIs) for the whole field and cloudy subset for Fields 1 and 2. Mean CVs are compared pairwise within a VI and the whole field or cloudy subset assessment. Values not sharing a letter are significantly different by Fisher's protected least significant different ($p \leq 0.05$).

	WHOLE FIELD				CLOUDY SUBSET			
	Field 1-1 (cloudy)		**Field 1-2 (sunny)**		**Field 1-1 (cloudy)**		**Field 1-2 (sunny)**	
NDVI	7.12	a	6.95	a	7.97	a	8.53	a
GNDVI	6.52	a	6.05	b	6.92	a	6.29	a
NDRE	12.9	a	11.9	b	12.0	a	12.4	a
MSAVI2	18.4	a	17.3	a	30.1	a	20.0	b
SR	34.4	a	34.1	a	36.4	a	36.2	a
	Field 2-1 (cloudy)		**Field 2-2 (sunny)**		**Field 2-1 (cloudy)**		**Field 2-2 (sunny)**	
NDVI	3.33	a	3.79	a	3.45	a	3.55	a
GNDVI	4.22	a	4.13	a	4.50	a	4.09	a
NDRE	8.20	b	8.65	a	7.99	b	8.62	a
MSAVI2	21.4	a	16.0	b	26.3	a	15.6	b
SR	28.3	a	27.9	a	29.3	a	27.0	b

Each normalized difference VI evaluated in this study – NDVI, GNDVI, and NDRE – is a ratio using relative differences in two bands. Additionally, SR is the ratio of reflectance in the NIR wavelength to the red wavelength. Several studies have determined that cloud cover only had a minimal effect on NDVI (Pinter et al., 1987; Bajwa and Tian, 2002) and SR (Pinter et al., 1987) because although reflectance in the red and NIR wavelengths did shift, they shifted together. For example, NIR reflectance values are 50% and 24% and the red reflectance values are 4% and 2% for non-cloudy and cloudy plots, respectively. The calculated NDVI values shown in Equations 2.2 and 2.3 remain approximately the same, regardless of the downward shift in reflectance values in individual bands.

Equation 2.2. Example calculation of NDVI for sunny conditions

$$NDVI = \frac{R_{NIR} - R_{red}}{R_{NIR} + R_{red}} = \frac{50 - 4}{50 + 4} = 0.85$$

Equation 2.3. Example calculation of NDVI for cloudy conditions

$$NDVI = \frac{R_{NIR} - R_{red}}{R_{NIR} + R_{red}} = \frac{24 - 2}{24 + 2} = 0.85$$

Due to the structure of the VI equations evaluated in this study, it can be surmised that the relative differences in reflectance values will compensate for any shaded areas. This is the reason that the whole image assessment as well as the subset assessment showed no major differences in NDVI, GNDVI, NDRE, or SR. Although these are some of the most commonly used VIs, there are others like MSAVI2 that do not use normalized relative differences. The formula for MSAVI2 is structured differently and was found to be more sensitive to cloud cover as witnessed by significant average and CV MSAVI2 differences in this study.

2.3.3 Effect of Cloud Cover on Reflectance

Several portions of the analysis highlighted differences in reflectance values in individual bands, as opposed to in the combination of bands, or VIs. Table 2.6 displays the average reflectance at each wavelength measured of Fields 1 and 2 for the whole image assessment and for the cloudy subset assessment. Field 1 showed no significant differences in any band. However, when assessing the subset of clouded plots, the average reflectance was significantly different in every measured band. Reflectance values in Field 2, which had considerably more cloud cover than Field 1, were significantly different in each measured band for the whole image and the cloudy subset. This indicates there is a downward shift in reflectance values at all bands measured when cloud cover is present.

Within plot variation in reflectance at the individual wavelengths measured were distinctly and significantly different in cloudy and sunny environments (Table 2.7). In Field 1, variation in reflectance was consistently higher when clouds were present. Field 2 also had higher variation with cloud cover, excluding reflectance in the blue (475 nm) and red (668 nm) wavelengths. In a ground-based study, Chang et al. (2005) also found that variation in reflectance increased with an increasing amount of clouds.

Table 2.6. Average reflectance values for the whole field and cloudy subset for Fields 1 and 2. Means are compared pairwise within a wavelength and the whole field or cloudy subset assessment. Values not sharing a letter are significantly different by Fisher's protected least significant different ($p \leq 0.05$).

	WHOLE FIELD				CLOUDY SUBSET			
	Field 1-1 (cloudy)		**Field 1-2 (sunny)**		**Field 1-1 (cloudy)**		**Field 1-2 (sunny)**	
Blue (475 nm)	2.63	a	2.70	a	1.65	b	2.98	a
Green (560 nm)	6.80	a	6.69	a	3.81	b	7.05	a
Red (668 nm)	3.62	a	3.76	a	1.98	b	4.42	a
Red Edge (717 nm)	18.6	a	18.5	a	9.21	b	18.9	a
NIR (840 nm)	49.4	a	50.8	a	23.5	b	49.2	a
	Field 2-1 (cloudy)		**Field 2-2 (sunny)**		**Field 2-1 (cloudy)**		**Field 2-2 (sunny)**	
Blue (475 nm)	1.44	b	2.38	a	0.988	b	2.38	a
Green (560 nm)	3.88	b	5.42	a	2.50	b	5.44	a
Red (668 nm)	1.45	b	2.24	a	0.854	b	2.23	a
Red Edge (717 nm)	11.7	b	16.8	a	6.99	b	16.9	a
NIR (840 nm)	44.3	b	64.4	a	26.5	b	64.9	a

Table 2.7. Average reflectance values for the whole field and cloudy subset for Fields 1 and 2. Means are compared pairwise within a wavelength and the whole field or cloudy subset assessment. Values not sharing a letter are significantly different by Fisher's protected least significant different ($p \leq 0.05$).

	WHOLE FIELD				CLOUDY SUBSET			
	Field 1-1 (cloudy)		**Field 1-2 (sunny)**		**Field 1-1 (cloudy)**		**Field 1-2 (sunny)**	
Blue (475 nm)	37.7	a	34.8	b	36.5	a	33.5	b
Green (560 nm)	34.0	a	31.6	b	35.8	a	31.4	b
Red (668 nm)	42.1	a	38.5	b	44.6	a	35.9	b
Red Edge (717 nm)	29.8	a	27.3	b	34.7	a	28.4	b
NIR (840 nm)	24.0	a	22.4	b	30.7	a	24.4	b
	Field 2-1 (cloudy)		**Field 2-2 (sunny)**		**Field 2-1 (cloudy)**		**Field 2-2 (sunny)**	
Blue (475 nm)	42.6	a	43.5	a	42.6	a	43.6	a
Green (560 nm)	36.3	a	35.4	b	36.9	a	35.3	b
Red (668 nm)	39.8	a	40.1	a	41.9	a	39.4	a
Red Edge (717 nm)	32.5	a	31.3	b	33.1	a	31.1	b
NIR (840 nm)	26.4	a	24.9	b	27.7	a	24.6	b

2.4 Conclusion

A brightness index (BI) was developed to more efficiently and easily delineate cloud cover in an image. Manually designated sunny plots averaged around 100% BI, while cloudy plots averaged approximately 50% BI. This technique could potentially be automated and used in situations where transient cloud cover is present during UAV data collection. Future research will be focused on combining multiple datasets from the same flight pattern that are conducted within a reasonable timeframe. This could potentially provide a quick and easy solution to UAV pilots that are conducting flights during summer months when cloud cover is common and fast-moving.

Cloud cover did impact the NDVI, GNDVI, and NDRE indices, but these effects were not consistent across both datasets and the differences captured would not likely be large enough to greatly impact management decisions based on reflectance. However, cloud cover did significantly affect the reflectance values in individual bands. The VIs mentioned are normalized relative difference ratios and appear to compensate for irradiance differences because the reflectance values utilized shift downward together, but this should not be assumed for all VIs. The formula for MSAVI2 is structured very differently from the other VIs evaluated in this study, and was significantly and substantially affected by cloud cover. Based on this analysis, a recommendation could be made to UAV users that cloud cover will not greatly affect normalized difference ratios such as NDVI, but efforts should be made to follow the camera or sensor manufacturer's protocol for atmospheric calibration. Other VIs that are not normalized difference ratios as well as reflectance in individual bands, such as NIR, should not be used to make agronomic management decisions when cloud cover is present in UAV imagery without proper and advanced shadow detection and removal.

2.5 Acknowledgements

The authors would like to acknowledge and thank Cotton Inc., Tennessee Cotton State Support, and Tennessee Soybean Promotion Board for funding this research.

2.6 References

Adeline, K., M. Chen, X. Briottet, S. Pang, and N. Paparoditis. 2013. Shadow detection in very high spatial resolution aerial images: a comparative study. *Journal of Photogrammetry and Remote Sensing,* 80: 21-38.

AUVSI. 2013. The economic impact of unmanned aircraft systems integration in the United States. Association for Unmanned Vehicle Systems International.

Bajwa, S. and L. Tian. 2002. Multispectral CIR image calibration for cloud shadow and soil background influence using intensity normalization. Applied Engineering in Agriculture 18(5): 627-635.

Bronson, K. F., J. D. Booker, J. W. Keeling, R. K. Boman, T. A. Wheeler, R. J. Lascano, and R. L. Nichols. 2005. Cotton canopy reflectance at landscape scale as affected by nitrogen fertilization. Agron. J. 97:654-660.

Chang, J., S. Clay, D. Clay, D. Aaron, D. Helder, and K. Dalsted. 2005. Clouds influence precision an accuracy of ground-based spectroradiometers. Communications in Soil Science and Plant Analysis 36: 1799-1807.

Gitelson, A. A. and M. N. Merzlyak. 1994. Quantitative estimation of chlorophyll using reflectance spectra. Journal of Photochemistry and Photobiology B: Biology, 22, 247–252.

Gitelson, A.A., Y.J. Kaufman, and M.N. Merzlyak, 1996. Use of a green channel in remote sensing of global vegetation from EOS-MODIS. *Remote Sens. Environ.,* 58: 289-298.

Gong, H. and D. Cosker. 2017. User-assisted image shadow removal. *Image and Vision Computing,* 62: 19-27.

Jordan, C. 1969. Derivation of leaf-area index from quality of light on the forest floor. Ecology 50(4): 663-666.

Lu, D., P. Mausel, E. Bronodizio, and E. Moran. 2004. Change detection techniques. *International Journal of Remote Sensing,* 25: 2365-2401.

Lukina, E., K. Freeman, K. Wynn, W. Thomason, R. Mullen, M. Stone, J. Solie, A. Klatt, G. Johnson, R. Elliott, and W. Raun. 2001. Nitrogen fertilization optimization algorithm based on in-season estimates of yield and plant nitrogen uptake. Journal of Plant Nutrition 24(6): 885-898.

Minu, S. and A. Shetty. 2015. A comparative study of image change detection algorithms in Matlab. *Aquatic Procedia* 4: 1366-1373.

Moges, S., K. Girma, R. Teal, K. Freeman, H. Zhang, B. Arnall, S. Holtz, B. Tubana, O. Walsh, B. Chung, and W. Raun. 2007. In-season estimation of grain sorghum yield potential using a hand-held optical sensor. Archives of Agronomy and Soil Science 53(6): 617-628.

Pinter P., H. Kelly, and S. Schnell. 1987. Spectral estimation of Alfalfa biomass under conditions of variable cloud cover. 18th Conference on Agricultural and Forest Meteorology. Sept. 14-18, 1987. American Meteorological Society. Boston, MA.

Qi, J., A. Chehbouni, A. Huete, Y. Kerr, and S. Sorooshian. 1994. A modified soil adjusted vegetation index. Remote Sens. Environ. 48: 119-126.

Radke, R., S. Andra, O. Al-Kofahi, and B. Roysam. 2005. Image change detection algorithms: a systematic survey. *IEEE Transactions on Image Processing* 14(3): 294-307.

Raper, T. B., J. J. Varco, and K. J. Hubbard. 2013. Canopy-based normalized difference vegetation index sensors for monitoring cotton nitrogen status. Agron. J. 105: 1345-1354.

Raper, T. and J. Varco. 2015. Canopy-scale wavelength and vegetative index sensitivities to cotton growth parameters and nitrogen status. Precision Agriculture. 16(1): 62-76.

Rouse, J. W., R. H. Haas, J. A. Schell, and D. W. Deering. 1973. Monitoring vegetation systems in the Great Plains with ERTS. Third Earth Resources Technology Satellite-1 Symposium. NASA Sp-351 I, Greenbelt, Maryland, USA pp. 09–317.

Simic Milas A., K. Arend, C. Mayer, M. Simonson, and S. Mackey. 2017. Different colours of shadows: classification of UAV images. *International Journal of Remote Sensing,* 38: 3084-3100.

Taylor, R. and J. Fulton. 2010. Sensor-based variable rate application for cotton. Precision Crop Management for Cotton. Cotton Inc. Cary, NC.

Xia, T., Y. Miao, D. Wu, H. Shao, R. Khosla, and G. Mi. 2016. Active optical sensing of spring maize for in-season diagnosis of nitrogen status based on nitrogen nutrition index. Remote Sens. 8, 605.

Yin, X. and M. McClure. 2013. Relationship of corn yield, biomass, and leaf nitrogen with normalized difference vegetation index and plant height. Agronomy Journal 105(4): 1005-1016.

Zhang, L., X. Sun, T. Wu, and H. Zhang. 2015. An analysis of shadow effects on spectral vegetation indexes using a ground-based imaging spectrometer. IEEE Geoscience and Remote Sensing Letters 12(11): 2188-2192.

CHAPTER 3 - DIURNAL EFFECTS ON UNMANNED AERIAL VEHICLE-ACQUIRED SPECTRAL REFLECTANCE DATA IN COTTON AND SOYBEAN PRODUCTION

Abstract

The use of unmanned aerial vehicles (UAVs) in remote sensing of agronomic crops has increased substantially. Spectral reflectance data is collected from a passive sensor mounted on a UAV, and is used to create vegetation index (VI) maps such as the normalized difference vegetation index (NDVI), normalized difference red edge index (NDRE), and the simple ratio (SR). These VI maps are then translated into spatial irrigation, fertilizer, or chemical management decisions. UAV users typically operate UAVs at the most convenient managerial time, regardless of current environmental conditions. The authors hypothesized that there is significant diurnal variability in reflectance values as well as the resulting NDVI, NDRE, and SR due to various spatio-temporal factors. Reflectance in the blue (475 nm), green (560 nm), red (668 nm), red edge (717 nm), and near-infrared (840 nm) wavelengths was collected at five different times throughout one day from one cotton research trial and one soybean research trial. Significant differences in NDVI, NDRE, and SR and in the individual wavelengths was found due to the time of day of data acquisition ($p \leq 0.05$). Preliminary user recommendations include avoiding data acquisition if dew is present, flying as close to 1200 h as feasible, and collecting data at the same time of day for each date of data acquisition if needed for crop tracking or phenotyping.

Keywords: UAV, UAS, agriculture, NDVI, NDRE, SR, vegetation index, diurnal, time

3.1 Introduction

Unmanned aerial systems have become an increasingly common method of acquiring spatial information in row crop agriculture. Sensors are mounted on unmanned aerial vehicle (UAV) platforms in order to collect spectral reflectance data from the crop in various wavelengths. Data is used in algebraic combinations to create a vegetation index (VI). Vegetation indices are indicative of plant stresses and thus can be used to inform management decisions regarding irrigation, fertilizer, or chemical applications (Gitelson and Merzlyak, 1994; Raper and Varco, 2015). The majority of UAV operations occur without regard to the time of day and environmental conditions present due to time constraints or limited education in the field of remote sensing (Hashimoto et al., 2019). Many commercially-available sensors claim to negate diurnal effects on data quality by providing atmospheric calibration. Some sensors have on-board spectroradiometers that measure incoming radiation and normalize reflectance values, while others provide an external calibration panel and protocol to perform a local, frequent calibration with known reflectance values.

The authors hypothesize that the time of day of UAV flight and data acquisition will have an effect on the data quality due to several spatio-temporal factors: the changing solar angle of incidence, heliotropic movement of certain agronomic crops, flight pattern of the UAV, and the presence of moisture on the crop. Other studies have been completed on the effect of these factors in other platforms, such as for satellite imagery (Nagol et al., 2015; Yuan and Elvidge, 1996; Schott et al., 1988), but limited studies have been completed with higher spatial resolution UAV-acquired imagery. Assmann et al. (2019) studied VI response to several environmental factors, and concluded that UAV users must be diligent and cautious in data collection so as to avoid major sources of error such as solar variation and cloud cover. Vega et al. (2015) found that time of UAV data collection had no effect on NDVI calculated imagery in a sunflower crop in a limited dataset. Reyniers (2003) discovered that while a change in light intensity did have an effect on the reflectance values in the individual bands, it did not affect the resulting NDVI. In contrast to those studies, Oliveira and Scharf (2015) measured reflectance from a cotton canopy throughout a day at several points within the growing season and found significant diurnal variability cause by external and internal plant factors. Similarly, Sticksel et al. (2004) observed significant diurnal effects on various vegetation indices. These studies represent the whole of the literature on this topic. The diurnal effect is

specific to crop and latitude and can be attributed and weighted differently to many factors (Hatfield and Pinter, 1993).

3.1.1 Potential Spatio-Temporal Factors

As previously noted, the authors hypothesize a diurnal effect on crop spectral reflectance collected from a UAV caused by several spatio-temporal factors. Most of the incoming radiation from sunlight is reflected directly back towards the angle of incidence, but some will be scattered in different directions (Holben and Justige, 1980). This phenomenon is referred to as bidirectional reflectance and is defined as the variation in reflectance due to changing angles of the sun, the crop canopy, and the sensor (Holben and Justige, 1980). Although row orientation, sun angle, and amount of ground cover can play a significant role, canopy architecture is the dominant factor affecting bidirectional reflectance (Jackson and Pinter, 1986; Ross and Marshak, 1989). Diurnal variability in bidirectional reflectance exists as the solar angle of incidence and the orientation of leaves changes throughout a day. Cotton and soybean plants, specifically, are heliotropic, meaning the leaves track the sun in order to maximize photosynthetic activity. This changing leaf orientation potentially introduces an additional source of error.

Another factor that could potentially influence reflectance values is the presence of water on the vegetation. Water can be present due to intercepted irrigation, precipitation, or dew. Dew is the condensation of moisture on leaves when the leaf surface temperature is at or below dew-point temperature (Sadler, 1996). Many studies have found that the presence of water on vegetation increases reflectance values (Fraser, 1994; Madeira et al., 2001). Pinter (1986) measured spectral reflectance in a dew-covered field and found that reflectance increased within the red band (0.65-0.69 μm), while NIR reflectance (0.76-0.9 μm) was not affected. This response to canopy wetness could influence data quality if data is collected when dew is present in the morning versus absent in the afternoon.

The flight pattern of the UAV for mapping purposes is generally a serpentine path, flying one direction then turning around 180 degrees on the next pass to return. This continuously changing direction of flight, and sensor location, could affect data if the sensor does not have on-board calibration. This error may be negated or emphasized through the post-process orthomosaic creation process. The orthomosaic

creation process consists of combining many individual images with overlap and sidelap to create a larger, composite orthomosaic used for data analysis.

Spectral reflectance data, or the resulting VIs, may be collected and used at one point in time to determine a specific application or management decision or data may be collected many times throughout a growing season for high throughput phenotyping or to monitor progress of the crop. The most commonly employed VI is the normalized difference vegetation index, or NDVI, (Rouse et al., 1973) shown in Table 3.1. NDVI was included in this analysis because it is the most commonly used VI in agriculture (Abdou et al., 1995) and because some studies have shown that although spectral response can shift in the red and near-infrared regions, they shift together such that NDVI is not affected (Reyniers, 2003; Vega et al., 2015). The normalized difference red edge index (NDRE) has more recently shown promise in mid-season assessments of crop nitrogen status (Raper and Varco, 2015) and is increasingly being utilized by UAV users. Although more commonly used with satellite imagery, the simple ratio (SR) is also included in this study to observe differences in a VI that does not have the same mathematical structure as NDVI and NDRE. Hashimoto et al. (2019) also observed NDVI and SR responses to variation in solar radiation and found that although these VIs use the same wavelengths, the SR is much more sensitive to changes in solar radiation.

Table 3.1. Vegetation indices (VIs) and formulas used in this study

Vegetation Index	Full Name	Formula	Reference
NDVI	Normalized difference vegetation index	$\frac{R_{NIR} - R_{Red}}{R_{NIR} + R_{Red}}$	Rouse et al., 1973
NDRE	Normalized difference red edge index	$\frac{R_{NIR} - R_{Red\,Edge}}{R_{NIR} + R_{Red\,Edge}}$	Gitelson and Merzlyak, 1994
SR	Simple ratio	$\frac{R_{NIR}}{R_{Red}}$	Jordan, 1969

This study was based on the desire to ensure that data is collected at a time of day when there is high data quality (i.e. collecting data once and making a sound management decision) and also high data stability (i.e. consistent data quality between collection dates when flying throughout the growing season). Because high data quality and stability are necessary, the objectives of this study were to determine if there is (1) a significant diurnal effect on VIs and overall spectral response and (2) the ideal timeframe in which a UAV should be used to collect spectral reflectance data.

3.2 Materials and Methods

Two agronomic crop trials, one in cotton (*Gossypium hirsutum,* L.*)* and one in soybeans (*Glycine max,* L.), were established at the University of Tennessee West Tennessee Research and Education Center in Jackson, TN (35°37'23.3"N, 88°50'47.5"W) in 2017 (Figure 3.1). Cotton treatments consisted of varying rates of nitrogen (N) from 0 to 120 lb N/ac at planting and approximately 50 days after planting (DAP). Eight treatments were replicated four times and arranged in a randomized complete block design. Plots consisted of six rows approximately 5.5 m wide by 9 m in length. The soybean trial evaluated effectiveness of various combinations of seed treatments. Twelve trial treatments were replicated four times and arranged in a randomized complete block design. Plots consisted of four rows approximately 3 m wide by 11 m in length. Both trials were oriented with rows planted northwest to southeast. Trial information is included primarily to signify that there are induced reflectance differences due to plant response to treatments, but is otherwise distinct from this study and trial results will not be presented in this manuscript.

3.2.1 Image Acquisition

A MicaSense RedEdge camera (MicaSense Inc., Seattle, WA) was attached in a nadir position to a custom quadcopter UAV for data collection. The multispectral camera captured one image per second in five narrow bands, described in Table 3.2. Bandwidth is defined as the width of the transmissivity curve at half of the peak transmissivity, or full width at half maximum (FWHM).

(a)



(b)



Figure 3.1. Research trial plots in (a) cotton and (b) soybeans at the University of Tennessee West Tennessee Research and Education Center used in this study. Plot polygons represent the experimental unit.

Table 3.2. MicaSense RedEdge camera specifications for band name, center wavelength (nm), and bandwidth (nm)

BAND	CENTER WAVELENGTH (nm)	BANDWIDTH (nm) at full width at half maximum (FWHM)
Blue	475	20
Green	560	20
Red	668	10
Red Edge	717	10
Near Infrared	840	40

An autonomous flight pattern at 120 m altitude was developed using the Mission Planner software (ArduPilot, Indianapolis, IN) for each crop trial and used in all flights. Flights occurred on August 9, 2017 at approximately 0800 h (8am), 1000 h (10am), 1200 h (12pm), 1400 h (2pm), and 1600 h (4pm) local time (GMT/UTC-5) for both trials. Solar noon, the time at which the sun is directly overhead, was determined to occur at approximately 1400 (2pm) at this location and date (NOAA Solar Calculator). Figure 3.2 and Table 3.3 describe the solar azimuth and elevation angle at each time of flight.

Protocol for the RedEdge camera specifies that the user take an image of a calibration panel, provided by the manufacturer, with known reflectance values immediately before and after a flight. When post-processing data to create image orthomosaics, this image is used to normalize all other data in an attempt to negate environmental effects. An on-board irradiance sensor is currently available for this camera, but was not available at time of data collection. Flight times were less than 5 minutes and partial cloud cover was observed during one flight; therefore, the authors are assuming that light conditions remained otherwise stable during data collection. Image mosaics were created by the MicaSense Atlas cloud-based service and downloaded in 16 bit GeoTIFF file format.

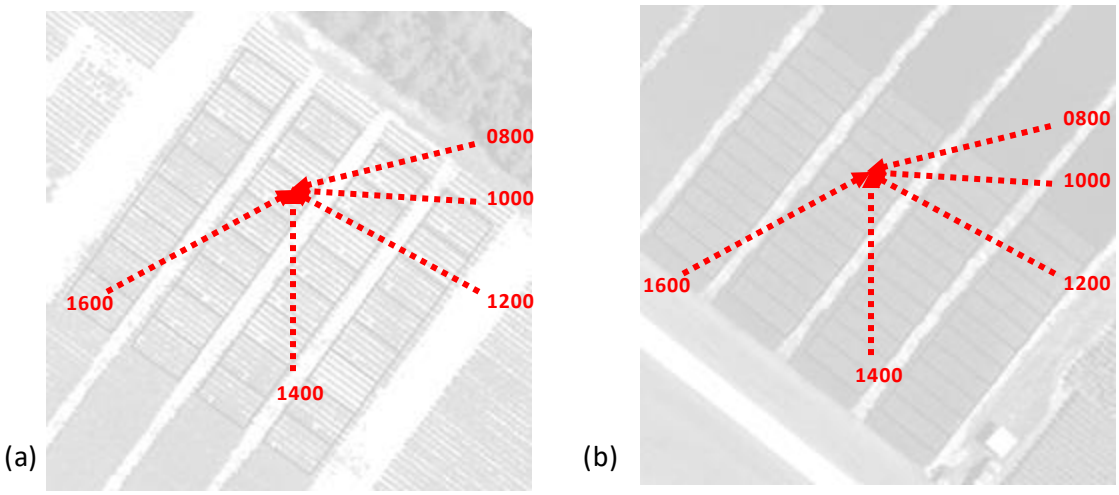


Figure 3.2. Solar azimuth at each time (h) of data acquisition in the (a) cotton and (b) soybean trials

Table 3.3. Solar azimuth and elevation angles at each time of data acquisition

TIME (h)	AZIMUTH(^{0})	ELEVATION (^{0})
0800	77	9
1000	94	33
1200	119	56
1400	179	70
1600	241	57

3.2.2 Image Analysis

Image analysis was completed in ArcMap 10.5 (ESRI, Redlands, CA). An isodata clustering algorithm, an unsupervised classification technique provided in ArcMap 10.5, was used to classify each pixel as vegetation or non-vegetation, comprised of soil and/or shadows. A histogram of each plot was created based on this classification to observe variation in non-vegetation pixels throughout the day. The non-vegetation pixels were then removed from each image so as to isolate the crop for further analysis. Spatial resolution of the resulting GeoTIFF orthomosaics was approximately 8 cm. Spatial comparisons between all time-series datasets required complete alignment of images, often referred to as image registration. Most UAVs use traditional global positioning system (GPS) or free differential correction services such as the Wide Area Augmentation System, or WAAS. Positional accuracy of WAAS is around 3m, which does not allow for complete image registration when comparing time-series images of the same field. Crop trials used for the study were in a small plot design (cotton 5.5 m by 9 m, soybean 3 m by 11 m), so individual plots were designated as the smallest experimental unit for comparisons. Plots were assigned the average and standard deviation of the reflectance and VI pixel values that were within each plot. Summarized data included reflectance values in each wavelength (blue at 475 nm, green at 560 nm, red at 668 nm, red edge at 717 nm, and near infrared at 840nm) and the calculated NDVI, NDRE, and SR. Further analysis was completed in Excel using the pivot table functionality to discover trends in the datasets. Plot data were subjected to analysis of variance in SAS (v9.5, SAS Institute, Cary, NC) to test for significance and means were separated using Fischer's protected least significant difference test at $P \leq 0.05$.

3.3 Results and Discussion

As would be expected, the amount of non-vegetation, i.e. shadows and soil, pixels in each image changed as a function of sun angle and cloud cover. Table 3.4 displays the percentage of shadows and soil in each image as a function of time. Note that the 1200 h flight in soybeans experienced partial cloud cover, but the remainder of the images for soybeans were all similar. Cotton was in an earlier growth stage and did not have a closed canopy (85 DAP) while the soybeans were at a later growth stage and did have a closed canopy (105 DAP) so limited soil was exposed. The most shadows and soil were visible at 0800 h in the cotton trial, followed by 1600 h, due to the solar azimuth and elevation angles as shown in Figure 3.2 and Table 3.3.

Table 3.4. Percentage non-vegetation (i.e. shadows and soil) present in each trial image at each time of data acquisition. Means were separated using Fischer's protected least significant difference test at P ≤ 0.05. *Soybean flight at 1200 h had a cloud covering most of the trial.

% SHADOWS AND SOIL IN IMAGES				
TIME (h)	**COTTON**		**SOYBEANS**	
0800	56.3	A	6.66	B
1000	32.5	C	2.84	B
1200	34.7	C	50.4*	A
1400	34.8	C	8.17	B
1600	38.9	B	4.06	B

Overall field averages for each VI and band wavelength were analyzed in order to isolate diurnal effect on said parameters. Generally, cotton and soybean VIs (Table 3.5) followed a parabolic trend with the highest VIs in the morning, decreasing around mid-day, then increasing again in late afternoon. All VI field averages were highest at the 0800 h flight, most likely due to the presence of dew on the leaves. Average VIs were lowest between 1000 h and 1200 h for the cotton trial and at 1200 h for the soybean trial, then increased at the 1400 h flight. Soybeans were more mature (around R6, 105 DAP) at the date of data acquisition than the cotton, and VI values were more saturated. Further studies should analyze and verify the diurnal effect on soybeans at an earlier growth stage.

Expounding on the variation in VI averages, individual study treatment VIs were also observed over the time period to ensure treatment differences were responding similarly to one another. Figure 3.3 displays NDVI, NDRE, and SR throughout the day for each treatment for both the cotton and soybean trials. Treatment descriptions are not included in this study, but some significant differences in VIs between treatments were observed. However, within each VI and trial, all treatments trended the same throughout the day.

Table 3.5. Overall normalized difference vegetation index (NDVI) values for each flight time and crop trial. Means were separated using Fischer's protected least significant difference test at P ≤ 0.05.

	COTTON						SOYBEANS					
TIME (h)	***NDVI***		***NDRE***		***SR***		***NDVI***		***NDRE***		***SR***	
0800	0.881	A	0.503	A	15.7	A	0.923	A	0.634	A	24.8	A
1000	0.851	C	0.482	C	12.7	C	0.893	B	0.529	C	17.6	B
1200	0.854	C	0.488	BC	12.9	C	0.845	D	0.486	E	11.8	E
1400	0.867	B	0.492	B	13.9	B	0.889	BC	0.538	B	17.0	C
1600	0.870	B	0.490	BC	14.4	B	0.885	C	0.507	D	16.5	D

In addition to the VI responses, it is also important to observe the diurnal effects on the individual bands, as well as the overall spectral response of the crop. Some producers and consultants might use a different VI than utilized in this study or use only the NIR value to make management decisions. Figure 3.4a and 3.4b display the reflectance at the individual band wavelengths for the cotton and soybean trials, respectively. In both trials, reflectance values were at, or near, the maximum collected values around 1200 h. This is most likely because the maximum intensity and highest angle of incoming light occurs at solar noon, while shadows are minimized. The reflectance values in the cotton trial generally increased from the earliest flight (0800 h), peaked around solar noon (1400 h), and decreased to the last flight (1600 h). The reflectance values from the soybean trial did not follow this same trend, but mostly had the lowest values at 0800 h and the highest values at the 1200 h or 1600 h flight.

Due to differing levels of reflectance in each band, it is difficult to discern the amount of variability within that band with respect to the mean. Figure 3.5 displays the coefficient of variation (CV) in the entire datasets, representing the disparity at which the reflectance at different wavelengths changes throughout a day. Reflectance in the NIR wavelength varied the least among its mean, while reflectance in the red wavelength varied the most as noted elsewhere in the literature (Kollenkark et al., 1982; Lord et al., 1989). This difference in variability in the red, red edge, and NIR regions can explain the significant diurnal effects on VIs seen in Table 3.5. Overall CV comparisons should not be made between trials as they were different crops under different research studies.

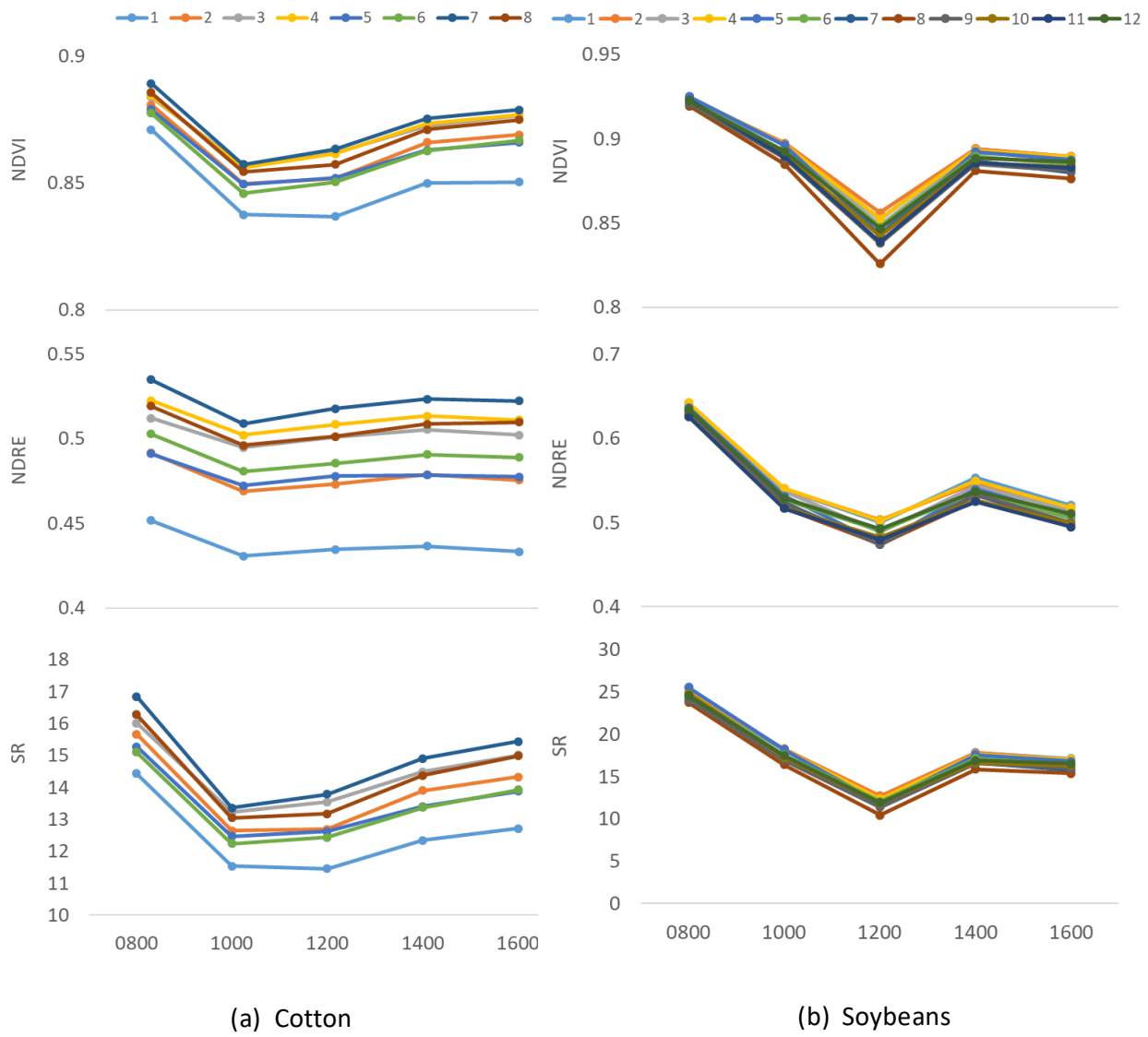


Figure 3.3. Variation in NDVI, NDRE, and SR throughout the day for each study treatment for the (a) cotton and (b) soybean trials

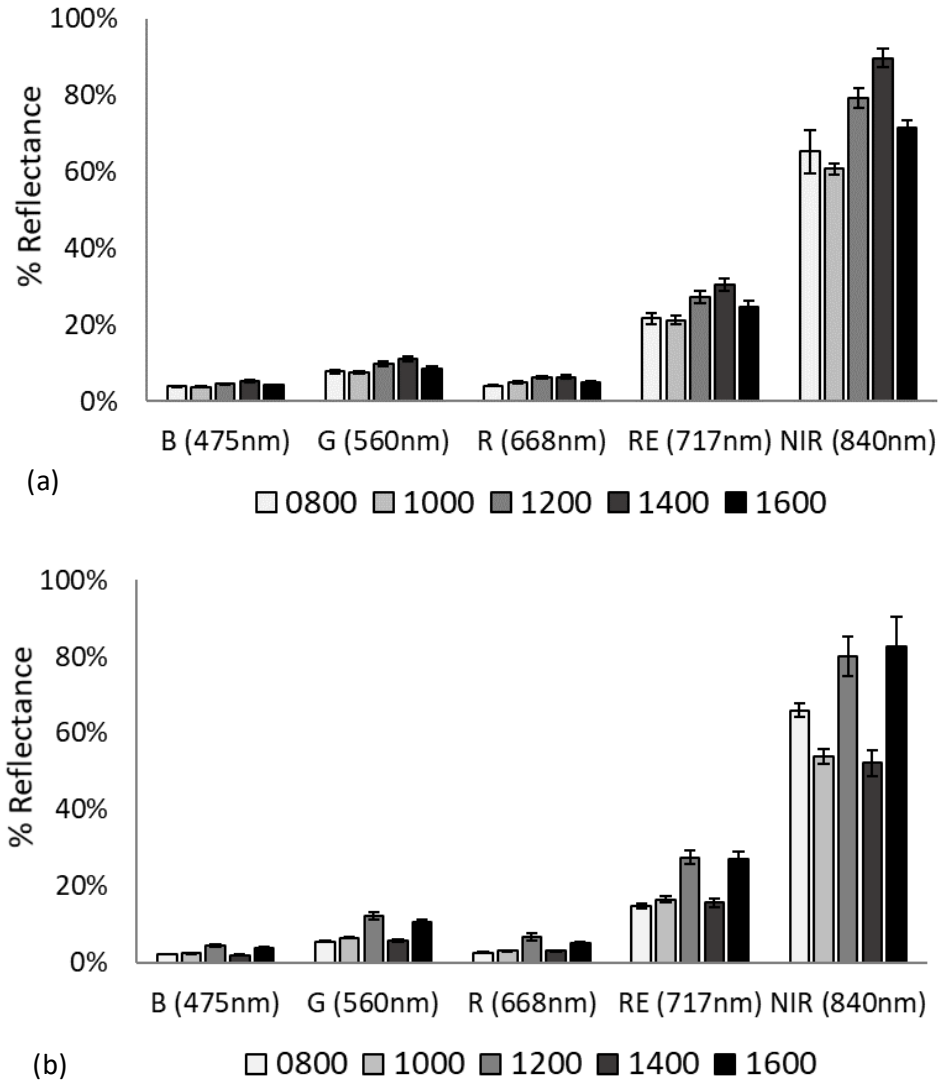


Figure 3.4. Reflectance values (%) in the blue (475 nm), green (560 nm), red (668 nm), red edge (717 nm), and near infrared (840 nm) wavelengths, separated by time of data acquisition for (a) the cotton trial and (b) the soybean trial.

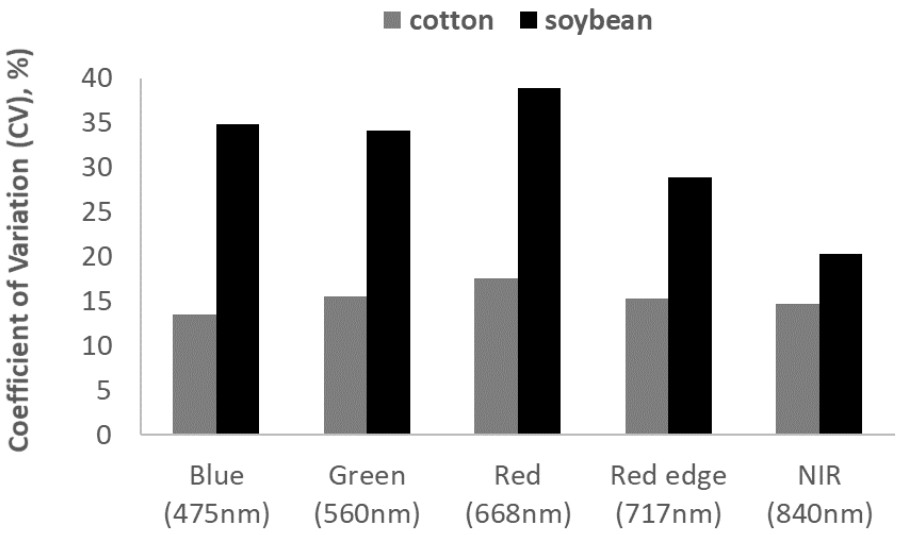
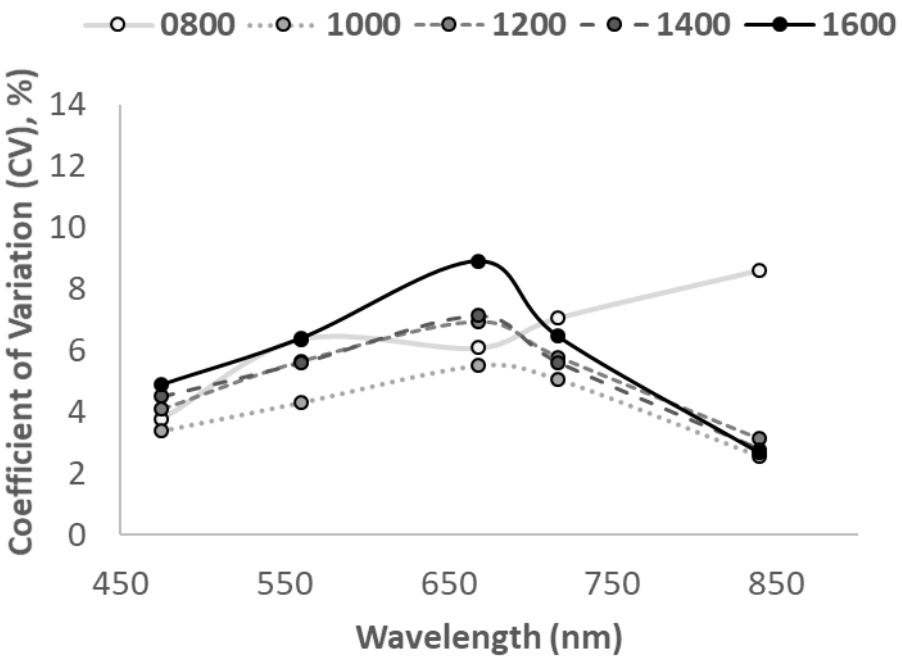


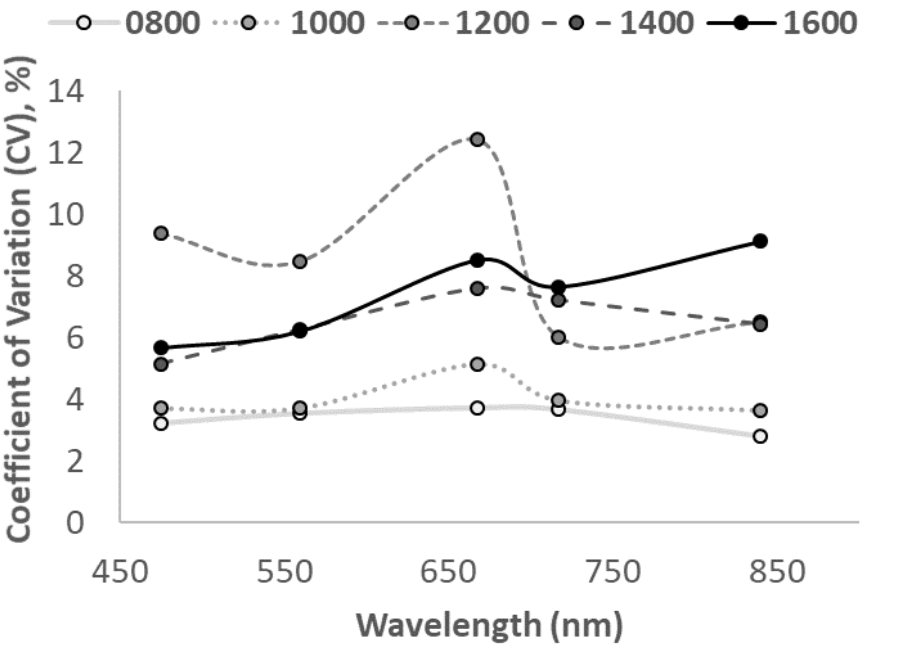
Figure 3.5. Coefficient of variation (CV, %) for the overall datasets for cotton and soybeans in the blue (475 nm), green (560 nm), red (668 nm), red edge (717 nm), and near infrared (840 nm) wavelengths, as well as for NDVI

Analyzing this further, variation between plots (or treatments) can also be seen in Figure 3.6a for cotton and Figure 3.6b for soybeans. For both trials, the highest amount of variability in reflectance values occurred between the 1200 h and 1600 h flights, indicating that more differences are being discerned between plots at these times, suggesting this to be the preferred time for data acquisition. In both trials, CV values trended similarly for all data acquisition times, except the flight at 0800 h when there was still dew present on the crop. Row orientation is the same within cotton and the soybean trials, but it should be noted that other studies have found a significant increase in diurnal variability in reflectance when rows are oriented north-south (Oliveira and Scharf, 2015).

Trends in VIs and individual bands were observed in this study, but the decision on what time of day to fly is still subjective as we do not know the true values. An active sensor, such as the GreenSeeker (Trimble Inc., Sunnyvale, CA), has its own light source and does not require the sunlight as do the UAV-mounted passive sensors. Further research could compare the active GreenSeeker sensor to a passive sensor on a UAV, although diurnal variability has also been found in cotton studies using GreenSeeker (Oliveira and Scharf, 2015). This indicates a diurnal physiological response, as opposed to an effect on spectral response.



(a)



(b)

Figure 3.6. Coefficient of variation among flight times (0800, 1000, 1200, 1400, and 1600 h) at blue (475 nm), green (560 nm), red (668 nm), red edge (717 nm), and near infrared (840 nm) wavelengths for the (a) cotton and (b) soybean trials

3.4 Conclusions

UAVs are increasingly being utilized to capture reflectance data in order to develop VIs such as NDVI, which is then being used to inform spatial management decisions. Environmental conditions during data acquisition, such as the time of day, are often ignored. Results from this study showed a significant diurnal effect on NDVI, NDRE, and SR as well as the overall spectral response of a cotton and soybean crop throughout a day. Future research is warranted to determine the best time of day to acquire data via UAV. This could be accomplished by the comparison of data acquired by an active sensor (stable, on-board light source) such as the GreenSeeker, to a passive sensor (sun as light source) such as the one used in this study.

The amount of shadows and soil present in the UAV images was at a minimum between 1000 h and 1400 h. Cotton VI values were similar and at their lowest at the 1000 h and 1200 h times, but were significantly different from the early and late afternoon times. Soybean VIs were at their lowest at the 1200 h time. Spectral variation in the studies was highest between 1200 h and 1600 h, signifying the most discernibility in agronomic differences. Accounting for all of these findings, this study points to the 1200 h time of data acquisition as being ideal. Preliminary recommendations include (1) avoiding the collection of spectral reflectance data early in the morning, (2) collecting UAV-acquired spectral reflectance data as close to 1200 h as possible and (2) if the application requires multi-temporal data collection, collecting data at the same time of day at each date of collection.

3.5 Acknowledgements

The authors would like to acknowledge and thank Tennessee Soybean Promotion Board and Tennessee Cotton State Support for funding this research.

3.6 References

Abdou, B., D. Morin, F. Bonn, and A. Huete. 1995. A review of vegetation indices. Remote Sensing Reviews 13: 95-120.

Assmann, J., J. Kerby, A. Cunliffe, and I. Myers-Smith. 2019. Vegetation monitoring using multispectral sensors – best practices and lessons learned from high latitudes. Journal of Unmanned Vehicle Systems 7(1): 54-75.

Fraser, A. B., 1994. The sylvanshine: retroflection from dew-covered trees. Applied Optics 33, 4539-4547.

Gitelson, A. and M. Merzlyak. 1994. Quantitative estimation of chlorophyll using reflectance spectra. Journal of Photochemistry and Photobiology B: Biology 22: 247–252.

Hashimoto, N., Y. Saito., M. Maki, and K. Homma. 2019. Simulation of reflectance and vegetation indices for unmanned aerial vehicle (UAV) monitoring of paddy fields. Remote Sens. 11, 2119.

Hatfield, J., and P. Pinter. 1993. Remote sensing for crop protection. Crop Protection 12(6), 403-413.

Holben, B. and C. Justige. 1980. The topographic effect on spectral response from nadir-pointing sensors. Photogrammetric Engineering and Remote Sensing 46: 1191-1200.

Jackson, R., and P. Pinter. 1986. Spectral response of architecturally different wheat canopies. Remote Sens. Environ. 20, 43-56.

Jordan, C. 1969. Derivation of leaf-area index from quality of light on the forest floor. Ecology 50(4): 663-666.

Kollenkark, J., V. Vanderbilt, C. Daughtry, and M. Bauer. 1982. Influence of solar illumination angle on soybean canopy reflectance. Applied Optics 21(7), 1179-1184.

Lord, D., R. Desjardins, and P. Dube. 1989. Sun-angle effects on the red and near-infrared reflectance of five different crop canopies. Can. J. Remote Sens. 14, 46-55.

Madeira, A., T. Gillespie, and C. Duke. 2001. Effect of wetness on turfgrass canopy reflectance. Agricultural and Forest Meteorology 107, 117-130.

Nagol, J., J. Sexton, D. Kim, A. Anand, D. Morton, E. Vermote, and J. Townshend. 2015. Bidirectional effects in Landsat reflectance estimates: is there a problem to solve? Journal of Photogrammetry and Remote Sensing. 103, 129-135.

Oliveira, L. and P. Scharf. 2015. Diurnal variability in reflectance measurements from cotton. Crop Science 54, 1769-1781.

Pinter, P. J. 1986. Effect of dew on canopy reflectance and temperature. Remote Sens. Environ. 19, 187-205.

Raper, T. and J. Varco. 2015. Canopy-scale wavelength and vegetative index sensitivities to cotton growth parameters and nitrogen status. Precision Agriculture. 16(1): 62-76.

Reyniers, M. 2003. Precision farming techniques to support grain crop production. PhD dissertation. Katholieke Universiteit Leuven, Faculty of Applied Bioscience and Engineering.

Ross, J., and A. Marshak. 1989. The influence of leaf orientation and the specular component of leaf reflectance on the canopy bidirectional reflectance. Remote Sens. Environ. 27, 251-260.

Rouse, J., R. Haas, J. Schell, and D. Deering. 1973. Monitoring vegetation systems in the Great Plains with ERTS. Third Earth Resources Technology Satellite – 1 Symposium. NASA Sp – 351 I, Greenbelt, MD, pp. 09-317.

Sadler, E. J., 1996. Considerations for determining leaf wetness using infrared thermometry in humid regions. Preprints 22nd conference on agricultural and forest meteorology 28 January – 2 February 1996. Atlanta, GA: American Meteorological Society, J6-J7.

Schott, J., C. Salvaggio, and W. Volchok. 1988. Radiometric scene normalization using pseudoinvariant features. Remote Sens. Environ. 26, 1-16.

Sticksel, E., J. Schachtl, G. Huber, J. Liebler, and F. Maidl. 2004. Diurnal variation in hyperspectral vegetation indices related to winter wheat biomass formation. Precision Agriculture 5(5): 509-520.

Vega, F., F. Ramirez, M. Saiz, and F. Rosua. 2015. Multi-temporal imaging using an unmanned aerial vehicle for monitoring a sunflower crop. Biosystems Engineering 132, 19-27.

Yuan, D., and C. Elvidge. 1996. Comparison of relative radiometric normalization techniques. Journal of Photogrammetry and Remote Sensing. 51, 117-126.

CHAPTER 4 - IN-SEASON ASSESSMENT OF COTTON NITROGEN STATUS FROM A HANDHELD SMARTPHONE AND AN UNMANNED AERIAL SYSTEM

Abstract

The widespread adoption of smartphones and unmanned aerial vehicles (UAVs) has the potential to ease collection of in-season cotton nitrogen (N) status. Subsequently, in-season cotton N status could be used to drive management decisions. The utility and limitations of these new platforms must be assessed and compared to current in-season measurements. The objectives of this study were to evaluate the ability of early and late season ground-based measurements to provide insight into cotton N status and to evaluate the ability of aerial-based measurements to correlate to ground-based measurements. While measurements failed to correlate strongly across seasons to leaf N, moderate relationships (R^2=0.453) between SPAD and DGCI were observed from late-season measurements. Poor relationships were found between early-season UAV- acquired vegetation indices (VIs) and leaf N. In an effort to minimize the use of time-consuming measurements, a linear relationship was established between soil plant analysis development (SPAD) meter readings and chlorophyll concentrations predicted by the dark green color index, or DGCI (R^2=0.711 ground-based, R^2=0.511 UAV-based). While additional site-years including aerial-based data are needed, this study demonstrates the usefulness of UAV-based reflectance data and VIs in predicting in-season cotton N status. Furthermore, it appears handheld DGCI measurements have the potential to replace SPAD for late in-season measurements of cotton N status.

Keywords: UAV, UAS, agriculture, vegetation index, SCCCI, red edge, DGCI, SPAD, NDVI

4.1 Introduction

Nitrogen (N) fertilization is a key, but fastidious component of sustainable cotton production. Deficiencies of N in cotton can lead to yield reductions and can harm overall productivity and profitability (Gerik et al., 1998; Read et al., 2006). Excessive N applications can lead to unwanted vegetative growth, increasing the need for plant growth regulator and insecticide applications, as well as increasing the difficulty of defoliation prior to harvest (Harris and Smith, 1980; Boman and Westerman, 1994). Unused N has an economic cost, as it provides no return on the input cost, and an environmental cost, as it has the potential to move offsite where it may contribute to environmental N pollution such as eutrophication (Carpenter et al., 1998). Nitrogen management in cotton has been heavily researched since the Haber-Bosch process was invented in the early 20th century. Current land grant university recommendations throughout the United States include optimal N rates as well as application timing, fertilizer source, and placement (Duncan and Raper, 2018; Lemon et al., 2009). Mid-season assessment of crop N status is an important method of determining whether the crop requirement has been met and the correct N rate to be applied at a time when the application can still have an effect on final yield (Gerik et al., 1998; Raper et al., 2013). Petiole and leaf analysis methods are typically used to determine crop N status, but these methods can be laborious, costly, and challenging to use in evaluation of spatial variability due to limits on scale (Buscaglia and Varco, 2002). One of the most popular methods of crop N assessment is the soil plant analysis development (SPAD) meter (Spectrum Technologies Inc., Aurora, IL), used as an indicator of chlorophyll concentration (Read et al., 2003) which decreases with N deficiency (Gerik et al., 1998). This method gives rapid results, but is still an in-situ method that is time-consuming and expensive.

Remote sensing of in-season crop N status is a promising method that can be performed quickly and relatively inexpensively. For decades, research has been conducted using handheld, tractor, airplane, and satellite mounted sensors (Rouse et al., 1973; Gitelson et al., 1996; Barnes et al., 2000; Raper et al., 2013). More recently, there has been increased interest in the use of unmanned aerial systems (UASs) to collect spectral information to determine crop N status (Ballester et al., 2017). Fertilizer application algorithms have been developed based on commercially available ground-based sensors (Arnal et al., 2008; Khalilian et al., 2017), but there is little information regarding the suitability of these algorithms to UAV-collected information. Tremblay et al. (2009) noted the non-transferability of application algorithms from one ground-based sensor to another, which could be extended intuitively to sensors on different platforms.

Many commercially available ground-based sensors use the normalized difference vegetation index (NDVI) as an indicator of crop N status, which has strong correlations in corn and wheat (Zubillaga and Urricariet, 2005; Ma et al., 1996; Stone et al., 1996). However, studies indicate a much weaker correlation between NDVI and cotton N status (Raper et al., 2013; Bronson et al., 2005). Several studies have indicated a stronger relationship between cotton N status and red-edge based vegetation indices (VIs) (Raper and Varco, 2015; Read et al., 2002). More recently, Ballester et al. (2017) found that the simplified canopy chlorophyll content index (SCCCI), also based on reflectance in the red edge region, was the most effective VI evaluated for predicting cotton N status when using a UAV. The dark green color index, or DGCI, was developed for use in turfgrass (Karcher and Richardson, 2003) then later extended to applications in corn (Rorie et al., 2011a; Rorie et al., 2011b) and cotton (Raper et al., 2012). This index uses hue, saturation, and brightness values from a digital image of a crop leaf against a color standard. Rorie et al. (2011a and 2011b) found a strong relationship between both SPAD and DGCI and corn leaf N. A few studies have indicated that DGCI also correlates well to cotton N status and chlorophyll concentrations (Raper et al., 2012; Wang et al., 2012). These studies each concluded that DGCI has the potential to provide an accurate assessment of N status in the crops evaluated by use of an inexpensive digital camera. These findings necessitate further investigation into the usefulness of and similarities between reflectance data and VIs developed from sensors mounted on ground and UAV platforms in estimating cotton N status. The objectives of this study were to (1) evaluate correlations in ground- and UAV-based measurements and VIs to cotton plant parameters, (2) evaluate the effectiveness of DGCI as an indicator of cotton N status, and (3) compare DGCI from ground- and UAV-based sensors.

4.2 Materials and Methods

Trials evaluating cotton (*Gossypium hirsutum,* L.*)* response to fertilizer N rate and fertilizer N timing were established during the 2016, 2017, and 2018 growing seasons at the University of Tennessee Research and Education Centers located in Milan (35°56'04.7"N 88°43'40.2"W), Jackson (35°37'23.3"N, 88°50'47.5"W), and Grand Junction (35°06'53.1"N 89°12'56.6"W), TN (Figure 4.1). Soil types at the Grand Junction, Jackson, and Milan locations are a Loring silt loam, Memphis silt loam, and Collins silt loam, respectively. The cotton cultivar DeltaPine 1522 B2XF (Bayer CropScience, St. Louis, MO) was planted in every site-year.



Figure 4.1. Cotton nitrogen (N) trial orthomosaics from (left to right): Milan 2016, Jackson 2017, and Ames 2017

Treatments (Table 4.1) consisted of four total N rates applied at different timings. All other agronomic management decisions were made in accordance with the University of Tennessee Extension Recommendations (Raper, 2016). All N was broadcast as ammonium nitrate with a handheld fertilizer spreader. Application A was applied after cotton had emerged but prior to reaching the early square stage. Application B was applied during the first week of flower. Treatment application timings were selected based on management practices common to the region.

Each treatment was replicated four times and arranged in a randomized complete block design. Each plot was six rows wide and 9 m in length. Row spacing at the Milan location was 1.01 m. Row spacing at Grand Junction and Jackson was 0.965 m. Planting, harvest, N application, and data collection dates are included in Table 4.2.

4.2.1 Ground-based Measurements

Plant measurements as described below were collected at the first week of flower since this timing is generally assumed to be the latest timing in which an application of N could be applied and still impact seed cotton yield (Gerik et al., 1998; Raper, 2015). Furthermore, previous research has indicated the very low N demand of the plant early during the growing season often prevents an accurate determination of N status before first flower (Gerik et al., 1998; Read et al., 2003). Additionally, in order to determine the N response at dates which N demand of each plant was substantial, a second ground-based data collection was conducted in 2016 at Grand Junction and Milan and in 2018 at the Jackson location.

Table 4.1. Treatments consisted of varied rates and timings of N; application A was made after emergence but prior to early square. Application B was made during the first week of flower.

Treatment #	Application A kg/ha	Application B kg/ha
1	0	0
2	45	0
3	90	0
4	135	0
5	22.5	22.5
6	45	45
7	67.5	67.5
8	0	90

Table 4.2. Planting, harvest, application, and data collection dates for each site-year.

Location	Year	Application A	Application B	Data Collection 1	Data Collection 2	Planting	Harvest
Grand Junction	2016	25-May	8-Jul	8-Jul	9-Aug	6-May	17-Oct
	2017	16-Jun	11-Jul	11-Jul	n/a	2-May	29-Sep
	2018	15-Jun	11-Jul	11-Jul	n/a	4-May	8-Nov
Milan	2016	6-Jun	7-Jul	7-Jul	8-Aug	24-May	28-Oct
Jackson	2017	16-Jun	20-Jul	20-Jul	n/a	16-May	26-Sep
	2018	15-Jun	10-Jul	10-Jul	27-Aug	3-May	19-Oct

Plant height, NDVI collected by a GreenSeeker handheld unit (Trimble Inc., Sunnyvale, CA), Soil Plant Analysis Development (SPAD) meter readings collected by a handheld SPAD 502 plus chlorophyll meter (Spectrum Technologies Inc., Aurora, IL), Dark Green Color Index (DGCI) readings from the FieldScout GreenIndex+ Nitrogen mobile application (Spectrum Technologies Inc., Aurora, IL), and leaf N content were collected at each data collection date. Plant height was manually collected from six plants within each plot. GreenSeeker NDVI was measured by walking the unit at 5 km hr^{-1} 0.762 m above row three and then row four of each plot. Five fully-expanded, mainstem leaves located five nodes below the apical meristem were then removed from each plot. Three SPAD measurements were immediately collected from each leaf and the leaf was then placed on the FieldScout GreenIndex+ color board. An Apple iPhone 6 (Apple Inc., Cupertino, CA) running the FieldScout Application (Spectrum Technologies Inc., Aurora, IL) was then used to collect an image of the leaf and determine DGCI. At every data collection, collected mainstem leaves were placed on ice for transport until they could be placed within driers. After drying, samples were ground to pass a 20-mesh sieve and leaf N concentration was determined by dry combustion (ELEMENTAR Rapid N, ELEMENTAR Analysensysteme, Hanau, Germany). Plots were harvested with either an automated weigh system outfitted on a Case 1822 picker (CNH Industrial America, LLC, Racine, WI) or with a plot bagging system outfitted on a John Deere 9900 picker (Deere & Company, Moline, IL). Seed cotton yield was collected from the center two rows of each 6 row plot.

4.2.2 Aerial Measurements

Aerial measurements were taken at a subset of the site-years. At the early-season collection dates in 2016 in Milan (7 July) and in 2017 in Grand Junction (11 July) and Jackson (17 July), a custom quadcopter UAV equipped with a MicaSense RedEdge (MicaSense Inc., Seattle, WA) camera, which collects spectral reflectance data one image per second in five narrow bands (Table 4.3), was flown over the trial. Autonomous flight plans were programmed in Mission Planner software (ArduPilot, Indianapolis, IN), with 80% overlap and sidelap at 120m altitude. In accordance to the MicaSense protocol, images of a manufacturer provided calibration panel were collected by the camera immediately prior to and after each flight. Calibration images, along with individual flight images, were uploaded into the cloud-based MicaSense Atlas (MicaSense Inc. Seattle, WA) service to create orthomosaics of the fields. Each resulting orthomosaic was downloaded in 16-bit GeoTIFF file format.

Table 4.3. MicaSense RedEdge camera specifications for band name, center wavelength (nm), and bandwidth (nm)

Band	Center Wavelength (nm)	Bandwidth (nm) at full width at half maximum (FWHM)
Blue	**475**	**20**
Green	**560**	**20**
Red	**668**	**10**
Red Edge	**717**	**10**
Near Infrared	**840**	**40**

4.2.3 Image Analysis

Image analysis of the orthomosaics was completed in ArcMap 10.5 (ESRI, Redlands, CA). Soil and shadowed areas were removed from the imagery using an unsupervised image classification technique that classified each pixel into either vegetation, soil, or shadow. Pixels classified as soil or shadow were removed in an effort to minimize the influence of non-vegetative or non-illuminated areas on data intended to make crop management decisions. Plots were delineated in the images and the average and standard deviation of each in-season and yield measurement was assigned to their respective plots for further analysis. The VIs in Table 4.4 were calculated using the plot-scale reflectance data collected by the UAV. Each VI was selected to capture commonly reported indices and indices which have been previously show to correlate strongly to cotton N status (Ballester et al., 2017; Raper and Varco, 2015; Wang et al., 2012).

In order to evaluate correlation of UAV-calculated DGCI to cotton N status, hue, saturation, and brightness values were calculated for each plot from UAV RGB reflectance using the equations provided by Karcher and Richardson (2003) and Rorie et al. (2011b). The DGCI was then calculated using the equation as described in Table 4.4. A color board was fabricated using a piece of plywood with 1 m diameter disks painted to color-match the Munsell standards used by Karcher and Richardson (2003). The color board was placed in the alleys of the plot studies where it could be seen by the UAV-mounted sensor. DGCI

Table 4.4. Selected vegetation indices (VIs) and corresponding references calculated within this study.

Vegetation Index	Equation	Reference
Normalized Difference Vegetation Index (NDVI)	$\frac{R_{NIR,840} - R_{R,668}}{R_{NIR,840} + R_{R,668}}$	Rouse et al., 1973
Green Normalized Difference Vegetation Index (GNDVI)	$\frac{R_{NIR,840} - R_{G,560}}{R_{NIR,840} + R_{G,560}}$	Gitelson et al., 1996
Normalized Difference Red Edge (NDRE)	$\frac{R_{NIR,840} - R_{RE,717}}{R_{NIR,840} + R_{RE,717}}$	Gitelson and Merzlyak, 1994
Simplified Canopy Chlorophyll Content Index (SCCCI)	$\frac{NDRE}{NDVI}$	Barnes et al., 2000; Raper and Varco, 2015
Dark Green Color Index (DGCI)	$\frac{\left[\frac{Hue - 60}{60} + (1 - Saturation) + (1 - Brightness)\right]}{3}$	Karcher and Richardson, 2003

values for each color board were calculated from each UAV flight and used in the calibration method described by Rorie et al. (2011a) to correct trial DGCI values.

Statistical analyses were conducted using JMP v14 (SAS Institute, Cary, NC). Seed cotton was considered to be a function of site-year, replication nested within site-year, fertilizer N rate, and fertilizer N timing. Pearson correlation coefficients were used to evaluate the association between in-season measurements and plant parameters. Yield data were subjected to analysis of variance in SAS (v9.5, SAS Institute, Cary, NC) to test for significance and means were separated using Fisher's protected least significant difference test at $p \leq 0.05$.

4.3 Results and Discussion

4.3.1 Ground-based Measurements

Observed cotton response to fertilizer N rate was weak at the early-season sampling dates (Table 4.5). While SPAD and DGCI measurements indicated significant differences existed between treatments, differences were slight. The 45 kg N/ha treatment resulted in significantly greater SPAD and DGCI readings than the untreated, but the untreated failed to separate from the 135 kg N/ha treatment and the 135 kg N/ha treatment resulted in significantly lower SPAD and DGCI readings than the 45 kg N/ha treatment. It is suspected this may be due to a temporary negative crop response from the excessive amount of N applied at the single early application timing. Plant height and GreenSeeker NDVI were not significantly impacted by fertilizer N rate. Leaf N increased significantly from the untreated to treated treatments, but no significant differences were noted between the 45, 90 and 135 kg N/ha rates. Leaf N content is generally evaluated as the true independent measure of plant N status as environmental conditions can affect how much of the applied fertilizer N is lost or taken up by the plant.

By the late-season sampling dates, observed cotton response to fertilizer N rate was much stronger (Table 4.6). SPAD readings increased significantly as fertilizer N rate increased. Leaf N and DGCI readings increased significantly from the untreated to the 45 kg N/ha rate and from the 90 kg N/ha to 135 kg N/ha rate, but significant differences were not noted between the 45 kg N/ha and 90 kg N/ha rates. In contrast,

while plant height of the untreated was significantly less than the 90 kg N/ha and 135 kg N/ha rates, significant differences were not noted between the untreated and 45 kg N/ha rate nor were significant differences noted between the 45 kg N/ha rate and the 90 kg N/ha or 135 kg N/ha rates. GreenSeeker NDVI increased significantly from the untreated to the treated treatments, but no separation between 45, 90, and 135 kg N/ha rates were observed.

Cotton response to fertilizer N timing was mixed. While leaf N and NDVI were not significantly impacted by delayed applications, SPAD readings decreased as applications were moved later into the season. In contrast, height was only significantly reduced when all fertilizer N was delayed to the flowering timing.

Relationships between leaf N and SPAD, DGCI, and NDVI from early and late season measurements are graphed in Figure 4.2. While coefficients of determination between leaf N and SPAD, DGCI and NDVI were all weak ($R^2 \leq 0.13$) during early season measurements, by the late season measurement timings strong relationships ($R^2 > 0.4$) were observed between leaf N and SPAD as well as leaf N and DGCI. Both relationships appeared to be quadratic, with coefficients of determination between leaf N and SPAD and leaf N and DGCI equaling 0.619 and 0.453, respectively. Nitrogen deficiency symptoms tend to be more visible and easier to measure later in the season as N demand is much higher as bolls are developing. However, this is generally too late to make a yield impacting fertilizer N application.

Table 4.5. Early-season (prior to 15 July) response of height, SPAD, DGCI, NDVI and leaf nitrogen (N) to applied fertilizer N rate averaged across site-year. Since measurements occurred prior to the second application timing, only data from the plots receiving all N fertilizer at the early application timing were included.

N Rate (kg/ha)	Height (cm)	SPAD	DGCI	NDVI	Leaf N (%)
0	78 ns[Z]	47.09 b	0.611 c	0.692 ns	3.52 b
45	81 ns	48.41 a	0.638 a	0.717 ns	4.35 a
90	81 ns	47.91 ab	0.632 ab	0.700 ns	4.64 a
135	77 ns	46.85 b	0.614 bc	0.680 ns	4.83 a

[Z]Values not sharing any letter within the same column are significantly different by the Fisher's protected least significant difference at the 5% level of significance.

Table 4.6. Late-season response (After 15 July) of height, SPAD, DGCI, NDVI and leaf nitrogen (N) to applied fertilizer N rate and timing averaged across site-year.

N Rate (kg/ha)	Height (cm)	SPAD	DGCI	NDVI	Leaf N (%)
0	86 b[Z]	46.73 d	0.613 c	0.641 b	2.59 c
45	92 ab	49.92 c	0.658 b	0.698 a	3.07 b
90	96 a	51.54 b	0.671 ab	0.697 a	3.30 ab
135	95 a	53.42 a	0.684 a	0.713 a	3.61 a
Timing					
Emergence	89 a	48.65 a	0.607 b	0.630 ns	2.63 ns
Split	89 a	46.45 b	0.633 a	0.648 ns	2.57 ns
Flowering	80 b	45.08 b	0.600 b	0.645 ns	2.57 ns

[Z]Values not sharing any letter within the same column are significantly different by the Fisher's protected least significant difference at the 5% level of significance.

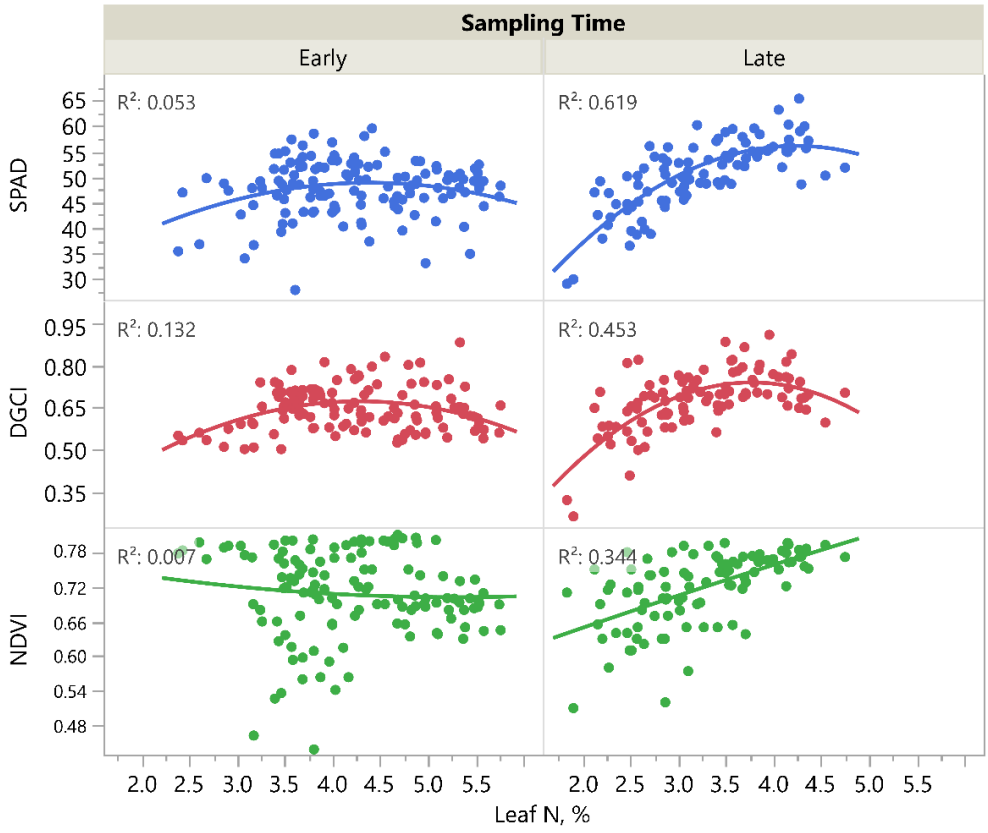


Figure 4.2. Relationships between leaf N and NDVI, DGCI, and SPAD graphed by sampling time, where the break between early and late is considered to be the second week of flower (typically 15 July).

Across all sampling dates, a moderate relationship (R^2=0.327) was observed between SPAD and DGCI (Figure 4.3). In contrast, no relationship was observed between NDVI and DGCI (R^2=0.055) and SPAD and NDVI (R^2=0.002). It is hypothesized the observed poor relationships are a function of NDVI's sensitivity to biomass compared to the relative lack of sensitivity of DGCI and SPAD to biomass.

4.3.2 Aerial-based Measurements

Significant differences were observed between the three site-years evaluated, thus correlations are provided independently by measurement and site-year in Table 4.7. Correlation between leaf N and all other measurements was mixed for 2016 Milan and 2017 Grand Junction. The 2017 Jackson sampling date (20 July) was prior to the second N application, but was fairly late and was considered as such in the analysis of ground measurements. It is notable that all ground-based and aerial measurements and VIs were highly correlated to leaf N at this later sampling date. This is in agreement with the ground-based analysis above, where correlations between leaf N and SPAD, DGCI, and NDVI were mixed early in the season and became stronger later in the season. Of the 5 wavelengths evaluated, all but NIR (840 nm) were significantly correlated to leaf N at the 2017 Jackson site ($p<0.01$) and at the 2017 Grand Junction site ($p<0.05$). Similar trends in wavelength correlation to mid-season cotton leaf N were found in a ground-based study by Raper and Varco (2015).

Plant height was significantly positively correlated with GreenSeeker NDVI at all three site-years. Many studies have noted that NDVI is a better indicator of plant biomass than plant N status (Li et al., 2001; Raper et al., 2013). Correlations with final seed cotton yield were conducted only with treatments 1-4 that did not receive a second N application. GreenSeeker NDVI and plant height were both significantly positively correlated to seed cotton yield at every site-year. All measured parameters, except NIR, were significantly correlated with final seed cotton yield at the 2017 Jackson site. Again, this is most likely due measurements being collected later as compared to the 2016 Milan and 2017 Grand Junction sites.

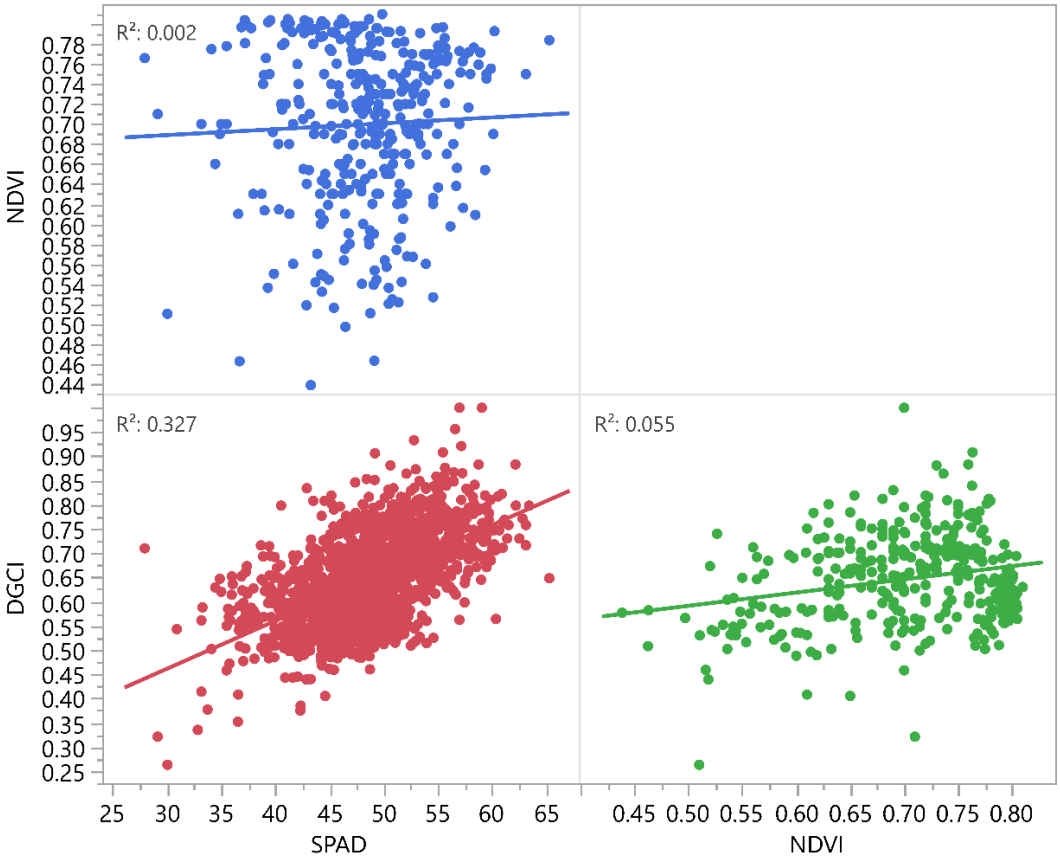


Figure 4.3. Relationships between SPAD, DGCI, and NDVI across early and late sampling times. Data from the late season 2016-Grand Junction site-year was excluded due to the severe drought stress present prior to that sampling date.

Table 4.7. Pearson correlation (r) values between specified plant parameters, vegetation indices, and individual wavelengths from ground-based sensors and UAV-based sensors from 2016 Milan, 2017 Grand Junction (GJ), and 2017 Jackson prior to Application B. Significance levels are denoted by ** p<0.01 and *p<0.05.

		Leaf N						Plant Height						Yield (only Trt 1-4)					
		2016 Milan		2017 GJ		2017 Jackson		2016 Milan		2017 GJ		2017 Jackson		2016 Milan		2017 GJ		2017 Jackson	
ground-based	SPAD	0.680	**	-0.224	ns	0.853	**	0.593	**	0.213	ns	0.405	*	0.526	*	-0.390	ns	0.614	*
	DGCI	0.434	*	-0.289	ns	0.578	**	0.443	*	0.112	ns	0.341	ns	0.232	ns	-0.345	ns	0.523	*
	NDVI	0.771	**	-0.095	ns	0.565	**	0.776	**	0.431	*	0.486	**	0.721	**	0.688	**	0.700	**
	Leaf N	-	-	-	-	-	-	0.845	**	-0.523	**	0.612	**	0.847	**	-0.170	ns	0.648	**
	Plant Height	0.845	**	-0.523	**	0.612	**	-	-	-	-	-	-	0.733	**	0.558	*	0.558	*
UAV-based	DGCI-corr	-0.290	ns	-0.515	**	0.696	**	-0.356	*	0.468	**	0.601	**	-0.269	ns	0.339	ns	0.867	**
	NDVI	-0.394	*	-0.539	**	0.761	**	-0.413	*	0.583	**	0.700	**	-0.331	ns	0.503	*	0.820	**
	NDRE	-0.404	*	-0.395	*	0.868	**	-0.352	*	0.638	**	0.598	**	-0.331	ns	0.582	*	0.762	**
	GNDVI	-0.471	**	-0.398	*	0.842	**	-0.431	*	0.608	**	0.598	**	-0.343	ns	0.561	*	0.806	**
	SCCCI	-0.373	*	-0.303	ns	0.849	**	-0.289	ns	0.619	**	0.547	**	-0.319	ns	0.584	*	0.724	**
	B	0.208	ns	0.567	**	-0.673	**	0.325	ns	-0.599	**	-0.618	**	-0.073	ns	-0.492	ns	-0.774	**
	G	0.263	ns	0.387	*	-0.779	**	0.329	ns	-0.621	**	-0.526	**	0.011	ns	-0.517	*	-0.788	**
	R	0.261	ns	0.586	**	-0.745	**	0.382	*	-0.607	**	-0.668	**	0.003	ns	-0.466	ns	-0.842	**
	RE	0.127	ns	0.386	*	-0.779	**	0.216	ns	-0.684	**	-0.500	**	-0.110	ns	-0.518	*	-0.726	**
	NIR	-0.222	ns	-0.327	ns	0.316	ns	-0.078	ns	0.402	*	0.328	ns	-0.603	*	0.571	*	0.090	ns

Both DGCI and the SPAD meter have been indicative of the concentration of chlorophyll in crops such as corn (Rorie et al., 2011b) and cotton (Read et al., 2003). Wang et al. (2012) developed a model to predict cotton chlorophyll content from DGCI data with a coefficient of determination of 0.88. This model was applied to both the ground- and UAV-based DGCI values in the current dataset and compared to SPAD measurements as the other indicator of plant chlorophyll content (Figure 4.4).

SPAD measurements were significantly correlated with both methods of predicting chlorophyll content, with the Pearson correlation coefficients (r) of 0.715 and 0.843 for the UAV- and ground-based DGCI values, respectively. The ground-based chlorophyll prediction (R^2=0.71) from this dataset is stronger than the UAV-based (R^2=0.51). This may be caused by additional noise in the UAV data obtained by the wider field of view. This dataset shows promise for the use of DGCI derived from early season ground- and UAV-collected RGB images to predict chlorophyll content.

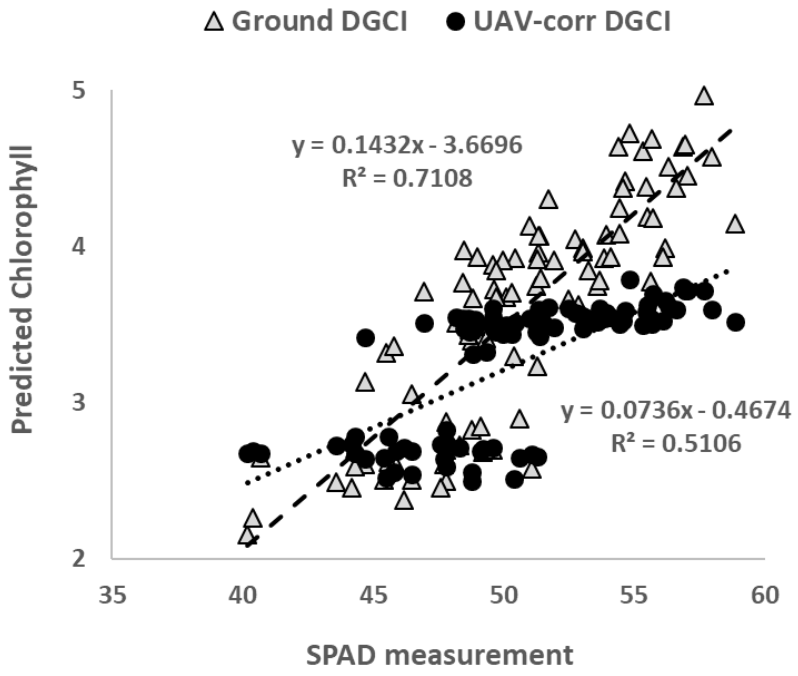


Figure 4.4. A regression of SPAD measurements to ground-based or UAV-based DGCI predictions of chlorophyll as modeled by Wang et al. (2012).

4.3.3 Seed Cotton Yield

Analysis of variance for seed cotton yield response to site-year, replication nested within site-year, fertilizer N rate, and fertilizer N timing is presented in Table 4.8. Response of seed cotton yield to fertilizer N rate is graphed by site-year in Figure 4.5. A significant increase in seed cotton yield was observed between the untreated and application rates of 45, 90 and 135 kg N/ha, but no significant differences were observed between rates of 45, 90 and 135 kg N/ha. A slight response of seed cotton yield to N applied can be seen in some site-years potentially due to the variability of soil residual N.

4.4 Conclusions

This study provides information to researchers, producers, and advisors on the utility and current limitations of in-season measurements of cotton N status. Correlations between leaf N and both ground- and UAV-based measurements were mixed to weak during the window of time in which a yield impacting fertilizer N application could be made. At later season sampling dates, strong relationships were noted between leaf N and SPAD and leaf N and DGCI. While this information will likely not be able to completely ameliorate N deficiencies within the current season, late season measurements could potentially provide valuable information to be used in subsequent seasons or direct partially ameliorating supplemental foliar N applications within the current season. Across all sampling dates and site-years, ground-based DGCI had a positive linear relationship with SPAD (R^2=0.327). Furthermore, early season DGCI from ground- (R^2=0.71) and aerial-based (R^2=0.51) images was successfully used to predict chlorophyll using a model developed by Wang et al. (2012). These findings indicate that DGCI could potentially be used as a replacement for SPAD in determining cotton N status.

Table 4.8. Analysis of variance (ANOVA) table for seed cotton yield response to site-year, replication nested within site-year, fertilizer nitrogen (N) rate, and fertilizer N timing.

Source	NPARM	DF	Sum of Squares	F Ratio	P>F
Site-year	5	5	73439238	61.0416	<.0001
Replication (Site-year)	18	18	21187967	4.892	<.0001
N Rate	3	3	3083549	4.2717	0.0062
Timing	2	2	1173352	2.4382	0.0905

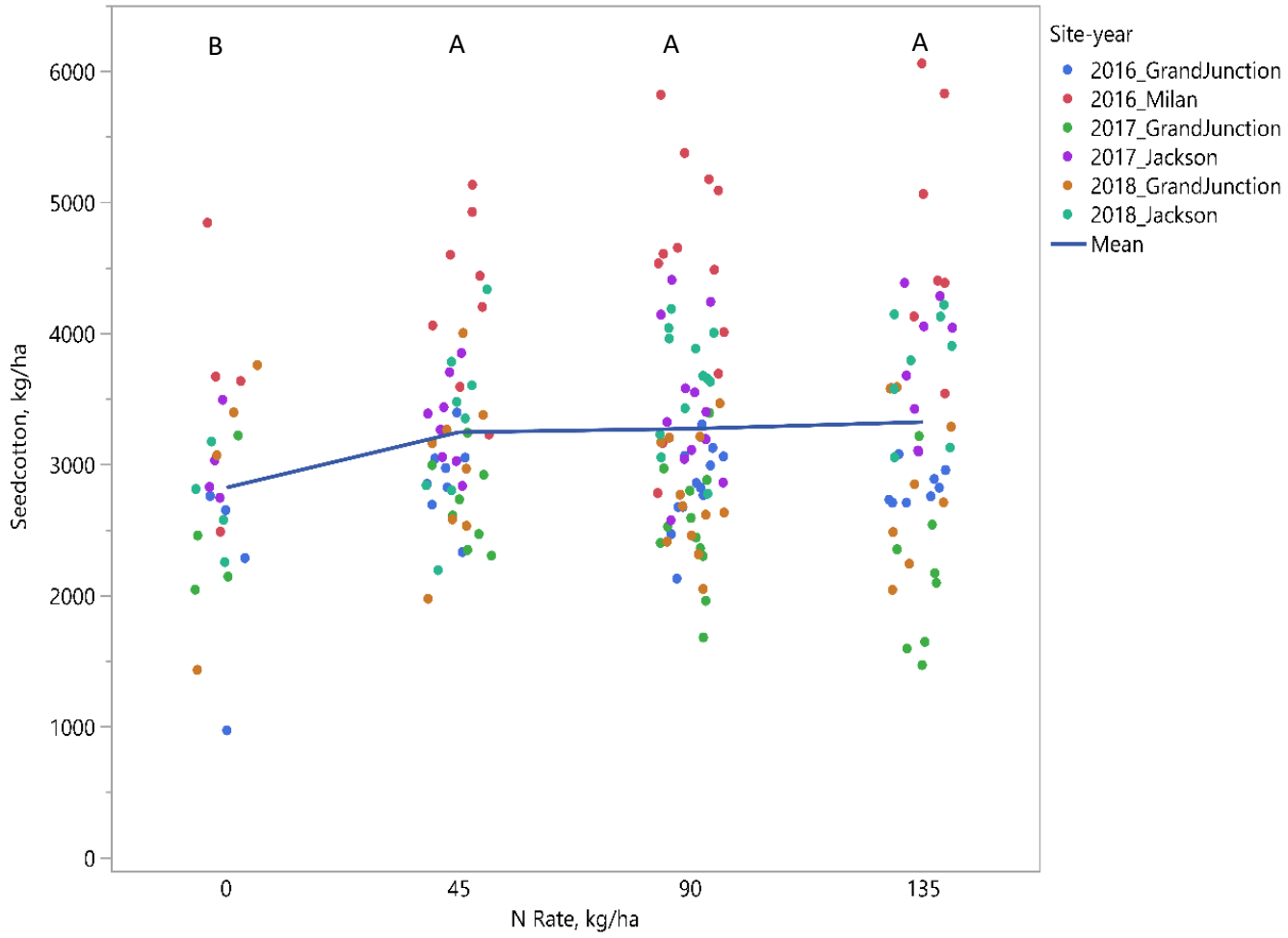


Figure 4.5. Response of seed cotton yield to fertilizer nitrogen (N rate) graphed by site-year. Rates not sharing any letter are significantly different by the Fisher's protected least significant difference at the 5% level of significance.

4.5 Acknowledgements

The authors would like to acknowledge and thank Cotton Inc. and Tennessee Cotton State Support for funding this research.

4.6 References

Arnal, B., R. Taylor, and B. Raun. 2008. The development of a sensor based nitrogen rate calculator for cotton. Proceedings of the Beltwide Cotton Conference, National Cotton Council of America, Memphis, TN.

Ballester, C., J. Hornbuckle, J. Brinkhoff, J. Smith, and W. Quayle. 2017. Assessment of in-season cotton nitrogen status and lint yield prediction from unmanned aerial system imagery. Remote Sens. 9, 1149.

Barnes, E., T. Clarke, S. Richards, P. Colaizzi, J. Haberland, M. Kostrzewski, P. Waller, C. Choi, E. Riley, T. Thompson, R. Lascano, H. Li, and M. Moran. 2000. Coincident detection of crop water stress, nitrogen status, and canopy density using ground based multispectral data. Unpaginated CD-ROM (13.pdf). *In* Proceedings of the 5th International Conference on Precision Agriculture, Bloomington, MN 16–19 July 2000. ASA, CSSA, and SSSA, Madison, WI.

Boman, R. and R. Westerman. 1994. Nitrogen and mepiquat chloride effects on the production of nonrank, irrigated, short-season cotton. Journal of Production Agriculture 7: 70-75.

Bronson, K. F., J. D. Booker, J. W. Keeling, R. K. Boman, T. A. Wheeler, R. J. Lascano, and R. L. Nichols. 2005. Cotton canopy reflectance at landscape scale as affected by nitrogen fertilization. Agron. J. 97:654-660.

Buscaglia, H. and J. Varco. 2002. Early detection of cotton leaf nitrogen status using leaf reflectance. Journal of Plant Nutrition 25 (9): 2067.

Carpenter, S., N. Caraco, D. Correll, R. Howarth, A. Sharpley, and V. Smith. 1998. Nonpoint pollution of surface waters with phosphorus and nitrogen. Ecological Applications 8(3): 559-568.

Duncan, L. and T. Raper. 2018. Cotton nitrogen management in Tennessee. *In* UT Extension W783. University of Tennessee Extension, Knoxville, TN.

Gerik, T., D. Oosterhuis, and H. A. Torbert. 1998. Managing cotton nitrogen supply. Advances in Agronomy 64: 115-147.

Gitelson, A. and M. Merzlyak. 1994. Quantitative estimation of chlorophyll using reflectance spectra. Journal of Photochemistry and Photobiology B: Biology 22: 247–252.

Gitelson, A., Y. Kaufman, and M. Merzlyak. 1996. Use of a green channel in remote sensing of global vegetation from EOS-MODIS. Remote Sensing of Environment 58: 289–298.

Harris, C. and W. Smith. 1980. Cotton production affected by row profile and N rates. Agron. J. 72(6): 919-922.

Karcher, D. and M. Richardson. 2003. Quantifying turfgrass color using digital image analysis. Crop Sci. 43: 943-951.

Khalilian, A., N. Rogers, P. Williams, Y. Han, A. Nafchi, J. Maja, M. Marshall, and J. Payero. 2017. Sensor-based algorithm for mid-season nitrogen application in corn. Open Journal of Soil Science 7: 278-287.

Lemon, R., R. Boman, M. McFarland, B. Bean, T. Provin, and F. Hons. 2009. Nitrogen management in cotton. *In* Texas A&M AgriLife Extension SCS-2009-1, College Station, TX.

Li, H., R. Lascano, E. Barnes, J. Booker, T. Wilson, K. Bronson, and E. Segarra. 2001. Multispectral reflectance of cotton related to plant growth, soil water and texture, and site elevation. Agron. J. 93: 1327-1337.

Ma, B., M. Morrison, and L. Dwyer. 1996. Canopy light r180eflectance and field greenness to assess nitrogen fertilization and yield of maize. Agron. J. 88(6): 915-920.

Raper, T., D. Oosterhuis, U. Siddons, L. Purcell, and M. Mozaffari. 2012. Effectiveness of the dark green color index in determining cotton nitrogen status from multiple camera angles. International Journal of Applied Science and Technology 2(1): 71-74.

Raper, T. B., J. J. Varco, and K. J. Hubbard. 2013. Canopy-based normalized difference vegetation index sensors for monitoring cotton nitrogen status. Agron. J. 105: 1345-1354.

Raper, T. 2016. 2015 Tennessee Cotton Quick Facts. *In* UT Extension W319. University of Tennessee Extension, Knoxville, TN.

Raper, T. and J. Varco. 2015. Canopy-scale wavelength and vegetative index sensitivities to cotton growth parameters and nitrogen status. Precision Agriculture. 16(1): 62-76.

Read, J., L. Tarpley, J. McKinion, and R. Reddy. 2002. Narrow-waveband reflectance ratios for remote estimation of nitrogen status in cotton. J. Environ. Qual. 31: 1442-1452.

Read, J., E. Whaley, L. Tarpley, and R. Reddy. 2003. Evaluation of a hand-held radiometer for field determination of nitrogen status in cotton. p.171-189. *In* Digital Imaging and Spectral Techniques: Applications to Precision Agriculture and Crop Physiology. ASA Special Publication 66, Madison, WI.

Read, J., R. Reddy, and J. Jenkins. 2006. Yield and fiber quality of Upland cotton as influenced by nitrogen and potassium nutrition. European Journal of Agronomy 24(3): 282-290.

Rorie, R., L. Purcell, D. Karcher, and A. King. 2011a. The assessment of leaf nitrogen in corn from digital images. Crop Science 51(5): 2174-2180.

Rorie, R., L. Purcell, M. Mozaffari, D. Karcher, C.A. King, M. Marsh, and D. Longer. 2011b. Association of "greenness" in corn with yield and leaf nitrogen concentration. Agron. J. 103: 529-535.

Rouse, J., R. Haas, J. Schell, and D. Deering. 1973. Monitoring vegetation systems in the Great Plains with ERTS. p. 9-317. Third Earth Resources Technology Satellite-1 Symposium. NASA Sp-351 I, Greenbelt, MD.

SAS. 1976. SAS v9.5. JMP14. SAS Institute, Cary, NC.

Stone, M., J. Solie, W. Raun, R. Whitney, S. Taylor, and J. Ringer. 1996. Use of spectral radiance for correcting in-season fertilizer nitrogen deficiencies in winter wheat. Trans. ASAE 39 (5): 1623– 1631.

Tremblay, N., Z. Wang, B. Ma, C. Belec, and P. Vigneault. 2009. A comparison of crop data measured by two commercial sensors for variable-rate nitrogen application. Precision Agriculture 10:145.

Wang, J., C. Wei, X. Wang, Q. Zhu, J. Zhu, and J. Wang. 2012. Estimation of chlorophyll contents in cotton leaves using computer vision based on gray board. Transactions of the Chinese Society of Agricultural Engineering 29(24): 173-180.

Zubillaga, M. and S. Urricariet. 2005. Assessment of nitrogen status in wheat using aerial photography. Communications in Soil Science and Plant Analysis 36: 13-14.

CHAPTER 5 – CONCLUSIONS AND USER RECOMMENDATIONS

5.1 Overview

The overarching objective of this dissertation is to ensure data quality and to enhance the utility of information collected by unmanned aerial systems (UASs) in agricultural crop production systems. Specifically, the objectives are to:

1. Identify environmental attributes that impact the stability of vegetation index (VI) maps derived from UAS-acquired data and develop recommendations for standard operating procedures
    a. Does shading from cloud cover affect VI maps? [Chapter 2]
    b. Does time of day of data acquisition affect VI maps? [Chapter 3]
2. Identify image acquisition and post-processing techniques to enhance the utility of VI maps derived from smartphone and UAS-acquired data [Chapter 4]

5.2 Chapter 2 Conclusions

A brightness index (BI) was developed to more efficiently and easily delineate cloud cover in an image. Manually designated sunny plots averaged around 100% BI, while cloudy plots averaged approximately 50% BI. This technique could potentially be automated and used in a situation where a transient cloud is present during UAV data collection. Future research will be focused on combining multiple datasets from the same flight pattern that are conducted within an hour. This could potentially provide a quick and easy solution to UAV pilots that are conducting flights during summer months when cloud cover is common and fast-moving.

Cloud cover did impact the NDVI, GNDVI, and NDRE indices, but these effects were not consistent across both datasets and the differences captured would not likely be large enough to greatly impact management decisions based on reflectance. However, cloud cover did significantly affect the reflectance values in individual bands. The VIs mentioned are normalized relative difference ratios and appear to compensate for irradiance differences because the reflectance values utilized shift downward together, but this should not be assumed for all VIs. The formula for MSAVI2 is structured very differently from the other VIs evaluated in this study, and was significantly and substantially affected by cloud cover. Based on this analysis, a recommendation could be made to UAV users that cloud cover will not greatly affect normalized difference ratios such as NDVI, but efforts should be made to follow the camera or sensor manufacturer's protocol for atmospheric calibration. Other VIs that are not normalized difference ratios

as well as reflectance in individual bands, such as NIR, should not be used to make agronomic management decisions when cloud cover is present in UAV imagery without proper and advanced shadow detection and removal.

5.3 Chapter 3 Conclusions

UAVs are increasingly being utilized to capture reflectance data in order to develop VIs such as NDVI, which is then being used to inform spatial management decisions. Environmental conditions during data acquisition, such as the time of day, are often ignored. Results from this study showed a significant diurnal effect on NDVI, NDRE, and SR as well as the overall spectral response of a cotton and soybean crop throughout a day. Future research is warranted to determine the best time of day to acquire data via UAV. This could be accomplished by the comparison of data acquired by an active sensor (stable, on-board light source) such as the GreenSeeker, to a passive sensor (sun as light source) such as the one used in this study.

The amount of shadows and soil present in the UAV images was at a minimum between 1000 h and 1400 h. Cotton VI values were similar and at their lowest at the 1000 h and 1200 h times, but were significantly different from the early and late afternoon times. Soybean VIs were at their lowest at the 1200 h time. Spectral variation in the studies was highest between 1200 h and 1600 h, signifying the most discernibility in agronomic differences. Accounting for all of these findings, this study points to the 1200 h time of data acquisition as being ideal. Preliminary recommendations include (1) avoiding the collection of spectral reflectance data early in the morning, (2) collecting UAV-acquired spectral reflectance data as close to 1200 h as possible and (2) if the application requires multi-temporal data collection, collecting data at the same time of day at each date of collection.

5.4 Chapter 4 Conclusions

This study provides information to researchers, producers, and advisors on the utility and current limitations of in-season measurements of cotton N status. Correlations between leaf N and both ground- and UAV-based measurements were mixed to weak during the window of time in which a yield impacting

fertilizer N application could be made. At later season sampling dates, strong relationships were noted between leaf N and SPAD and leaf N and DGCI. While this information will likely not be able to completely ameliorate N deficiencies within the current season, late season measurements could potentially provide valuable information to be used in subsequent seasons or direct partially ameliorating supplemental foliar N applications within the current season. Across all sampling dates and site-years, ground-based DGCI had a positive linear relationship with SPAD (R^2=0.327). Furthermore, early season DGCI from ground- (R^2=0.71) and aerial-based (R^2=0.51) images was used to predict chlorophyll using a model developed by Wang et al. (2012). These findings indicate that DGCI could potentially be used as a replacement for SPAD in determining cotton N status.

5.5 User Recommendations

Based on findings in Chapters 2-4, UAV pilots collecting imagery for agricultural management should ensure data quality and stability by:

- Cautiously collecting reflectance data in the presence of cloud cover. If clouds will be present, only use difference vegetation ratios, such as NDVI or NDRE, instead of other algebraically-structured VIs or reflectance in individual bands, such as NIR.
- Avoid collection of reflectance data when moisture is present on the crop. Collect data as close to noon as possible. If there is a desire to compare multiple datasets throughout a growing season, ensure the data is collected around the same time of day to minimize diurnal effects.

5.6 Future Research

Conclusions from Chapter 2 confirm that clouds have a significant effect on multispectral reflectance data. Future research will be focused on combining multiple datasets from the same flight pattern that are conducted within a reasonable timeframe. This could potentially provide a quick and easy solution to UAV pilots that are conducting flights during summer months when cloud cover is common and fast-moving. Results from Chapter 3 showed a significant diurnal effect on NDVI, NDRE, and SR as well as the overall spectral response of a cotton and soybean crop throughout a day. Future research is warranted to determine the best time of day to acquire data via UAV. This could be accomplished by the comparison of

data acquired by an active sensor (stable, on-board light source) such as the GreenSeeker, to a passive sensor (sun as light source) such as the one used in this study.

Chapter 4 indicated that DGCI could potentially estimate cotton N status in-season and serve as a replacement for SPAD. Additional site-years in different environments are warranted to fully explore the potential for this index in cotton production.

VITA

Lori Duncan was raised in Sevier County, Tennessee. She graduated with both her bachelors of science and masters of science in Biosystems Engineering from the University of Tennessee in 2010 and 2012, respectively. Lori was hired by the University of Tennessee Extension in 2012 as an Extension Specialist, where she continues to be employed. She began her doctoral studies in 2013 and is completing the degree in December 2019.